# An extension of the Boussinesq-type models to weakly compressible flows

Gaël Richard

Version of Record: https://www.sciencedirect.com/science/article/pii/S0997754621000832
Manuscript_8b0a5cb1eec3e90df06acbac7b81b779

# An extension of the Boussinesq-type models to weakly compressible flows

Gaël L. Richard[a,*]

[a] *Univ. Grenoble Alpes, INRAE, UR ETNA, 38000 Grenoble, France*

**Abstract**

An extension of the Boussinesq-type models to weakly compressible flows is derived in the fully nonlinear case. The dispersive properties are consistent with the linear theory of compressible fluids at the long-wave limit. The particular case of a vanishing Mach number gives a quasi-incompressible model, intended for coastal wave simulations, which is a hyperbolic version of the Serre-Green-Naghdi equations, with a new treatment of the bathymetric terms. Both the compressible and quasi-incompressible models are hyperbolic four-equation models on an arbitrary bathymetry, with an exact equation of energy conservation. In addition, these models are extended to hyperbolic and fully nonlinear five-equation versions with improved dispersive properties. A remarkable property of the quasi-incompressible model with improved dispersive properties is that it is possible to decrease significantly the sound velocity, and thus the computational time, with the same accuracy or even slightly better. The numerical results show good agreement of the quasi-incompressible model with experimental data and the capability of the compressible model to calculate the decrease of tsunami velocity due to compressible effects.

*Keywords:* Boussinesq-type models, coastal waves, tsunamis, compressibility, Serre-Green-Naghdi equations

## 1. Introduction

Boussinesq-type models are commonly used for water wave simulations if the shallow-water – or long-wave – assumption holds, which is the case for coastal waves or for tsunami propagation. The original Boussinesq model (Boussinesq 1872 [1]) was derived for a constant depth. It was extended by Peregrine (1967) [2] to the case of a variable bathymetry. The Boussinesq model is weakly nonlinear, which means that the nonlinearity parameter, defined by the ratio of the wave amplitude to the water depth, is small. This assumption entails some discrepancies, notably in the case of coastal waves where the nonlinearity can increase to $O(1)$. A fully nonlinear model was first derived by Serre (1953) [3] (see also Su & Gardner 1969 [4]) in the one-dimensional (1D) case and extended to the two-dimensional (2D) case by Green and Naghdi (Green *et al.* 1974 [5], Green & Naghdi 1976 [6]). This model, called thereafter the Serre-Green-Naghdi model, can be derived from the Euler equations as an asymptotic model in the shallow-water regime without any assumption on the wave amplitude (Lannes 2013 [7]). Even when such models are fully nonlinear, the shallow water hypothesis (the depth is small compared to the wavelength) implies that they are weakly dispersive (see for example Kirby 2016 [8]). The dispersion relation of the Airy wave theory is recovered if $kh \ll 1$ where $k$ is the wave number and $h$ the water depth.

Many works have been proposed that aimed to extend the validity domain of the Boussinesq-type models to larger depths or shorter wavelengths with respect to their dispersive properties, in a weakly nonlinear case (Madsen & Sørensen 1992 [9], Nwogu 1993 [10]) or in the fully nonlinear case (Wei *et al.* 1995 [11], Kennedy *et al.* 2001 [12], Bonneton *et al.* 2011 [13], Chazel *et al.* 2011 [14]). Models based on higher-order expansions were derived by Agnon *et al.* (1999) [15], Gobbi *et al.* (2000) [16] and Madsen *et al.* (2002) [17]. An alternative to the high-order series expansions is the multi-layer approach (Lynett & Liu 2004 [18], Liu *et al.* 2018 [19]). The reader is referred to Brocchini (2013) [20] and Kirby (2016) [8] for a review of Boussinesq-type models.

The Boussinesq-type models can be derived by averaging over the water depth the fundamental mass and momentum equations of fluid mechanics. As a result, the dimension of the system is reduced by one; a 2D-flow is modelled by a 1D-system of equations and a three-dimensional (3D) flow reduces to a 2D-model. Furthermore the boundary conditions at the bottom and at the free surface are incorporated in the model equations. The computational time for a numerical simulation is thus greatly reduced. However the numerical resolution is confronted with two important problems. The first problem is the presence of high-order derivatives in the equations which are not easy to handle numerically. In particular, the Serre-Green-Naghdi equations feature third-order derivatives, and some Boussinesq-type models with improved dispersive properties include fifth-order derivatives. The second problem is that an elliptic step has to be solved at each time step

*Corresponding author.
E-mail address: gael.richard@inrae.fr

of the numerical resolution. Both problems result from the assumption of incompressibility which creates a non-local effect because pressure variations propagate at infinite celerity in an incompressible fluid. The pressure satisfies an elliptic Poisson equation which is the mathematical expression of this non-locality. In the depth-averaged models of the Boussinesq-type, the non-locality entails also an elliptic step which is time-consuming because a global linear system has to be solved at each time step. Moreover the resolution of the linear system adds complexity for the implementation of parallelization techniques which are often necessary to reduce the computation time.

A solution of these problems is to use a hyperbolic approximation of the Boussinesq-type models. The first hyperbolic model of this type was proposed by Antuono *et al.* (2009) [21]. Favrie & Gavrilyuk (2017) [22] derived a hyperbolic approximation of the Serre-Green-Naghdi equations for a constant bathymetry with a variational method using an augmented Lagrangian leading to an unconditionally hyperbolic system giving the Serre-Green-Naghdi system when a parameter of the new system goes to infinity. This method reduces greatly the computational time. A mathematical justification of this approximation was given by Duchêne (2019) [23]. Another hyperbolic approximation was derived by Escalante *et al.* (2019) [24] for an arbitrary bathymetry with the method of an artificial compressibility. This approach was extended by Escalante & Morales de Luna (2019) [25] who obtained a hyperbolic approximation covering several classical Boussinesq-type models. A hyperbolic approximation of the Serre-Green-Naghdi equation with an exact energy conservation equation was proposed by Bassi *et al.* (2020) [26]. In all these approaches, the case of an arbitrary bathymetry is handled by a six-equation model instead of a four-equation model for a constant depth. The hyperbolic system may be seen as a relaxation of the original non-hyperbolic system. It is based on a modified system in which the divergence constraint on the velocity field is coupled with the other conservation laws and, in particular, with a transport equation for the non-hydrostatic pressure, including a relaxation term on the depth-averaged vertical velocity which introduces a high but finite velocity. At the limit where this velocity goes to infinity, the original non-hyperbolic system is recovered.

These approaches are related to the general method of taking into account the compressibility and the propagation of acoustic waves in order to avoid the resolution of a global system at each time step. This method is used in atmospheric numerical models for a long time (see for example Hill 1974 [27], Klemp & Wilhelmson 1978 [28], Skamarock & Klemp 1992, 2008 [29, 30]) and in non-hydrostatic ocean models (Auclair *et al.* 2018 [31]). The drawback of this method is that the very high value of the sound velocity (around 1500 $\mathrm{m{\cdot}s^{-1}}$ in water) severely restricts the time step. This problem can be solved by using an artificially smaller sound velocity, adding thus an artificial compressibility, leading to a system which is sometimes called pseudo-compressible (Auclair *et al.* 2018 [31]). The same method is used for the hyperbolic approximations of the Boussinesq-type models where the large parameter giving the original non-hyperbolic system at the infinite limit is chosen as small as possible to give the same results as the incompressible system at an excellent approximation while keeping the time step to a reasonably small value.

In these approaches the compressibility and the acoustic waves are included purely to facilitate and accelerate the numerical solution process. The hyperbolic models were conceived as hyperbolic approximations of the incompressible non-hyperbolic Serre-Green-Naghdi or Boussinesq-type models. The goal was to obtain nearly the same solutions with a hyperbolic structure to remove the high-order derivatives and the elliptic step. Compressible effects are for most cases negligible because of the usually very small value of the Mach number.

However compressibility can have important and measurable effects in the case of tsunamis. Standard models for tsunami propagation predict arrival times which are systematically too early compared to the observations. The delay is significant and can reach several minutes in the far field (see for example Yamazaki *et al.* 2012 [32], Grilli *et al.* 2013 [33], in the case of the 2011 Tohoku-oki event). This discrepancy is attributed to two main effects which are the compressibility of seawater and the elasticity of the solid earth (Tsai *et al.* 2013 [34], Allgeyer & Cumins 2014 [35], Baba *et al.* 2017 [36], Abdolali & Kirby 2017 [37]). Although a tsunami in a deep ocean is nevertheless a shallow-water flow because the order of magnitude of its wavelength (about 100 km) is much larger than the ocean depth (4 000–6 000 m), the Mach number defined by the ratio of the incompressible surface wave celerity $\sqrt{gh}$, where $g$ is the gravity acceleration, to the sound speed is of the order of 0.13–0.16 which leads to a decrease in phase speed of about 0.5 % (Abdolali *et al.* 2019 [38]) which can explain an important part of the observed discrepancy. The capability to accurately model tsunami propagation with precise calculation of arrival time is essential for the study of these phenomena, in particular for the determination of source and earth properties using the inverse problem, and for early warning systems (Baba *et al.* 2017 [36], Abdolali *et al.* 2019 [38]). In the latter case a low computational cost is also crucial for an efficient real-time system.

Various methods have been implemented to take into account this compressibility effect and the earth elasticity effect (Tsai *et al.* 2013 [34], Allgeyer & Cummins 2014 [35], Watada 2014 [39], Baba *et al.* 2017 [36], Abdolali & Kirby 2017 [37], Abdolali *et al.* 2019 [38]). Boussinesq-type models are useful in modelling tsunamis propagation because they include dispersive effects which can be important (Grilli *et al.* 2013 [33], Kirby *et al.* 2013 [40], Glimsdal *et al.* 2013 [41]). However a Boussinesq-type model with compressibility effects is still lacking.

In this paper a fully nonlinear hyperbolic Boussinesq-type model with compressibility effects is derived. This is

the first extension of the Boussinesq-type models to compressible flows. A particular case of this model is obtained when the Mach number goes to zero. This leads to a quasi-incompressible version, which is a hyperbolic approximation of the Serre-Green-Naghdi model.

The compressible model is derived in §2 with a new treatment of the bathymetric terms which enables to model the case of an arbitrary bathymetry with only four equations instead of six, with an exact equation of energy conservation. The hyperbolicity, the dispersive properties and the soliton solutions are studied in §3.

A model with improved dispersive properties is derived in §4. This is a five-equation model, including on an arbitrary bathymetry. This is the first hyperbolic Boussinesq-type model with improved dispersive properties which is fully nonlinear. To the author's knowledge, the only other hyperbolic Boussinesq-type model with improved dispersive properties is the seven-equation model derived by Escalante & Morales de Luna (2020) [25], which is a hyperbolic approximation of the weakly nonlinear model of Madsen & Sørensen (1992) [9].

A remarkable property of the quasi-incompressible model with improved dispersive properties is that it is possible to decrease artificially the sound velocity, and consequently the computational time, much more than for the model with standard dispersive characteristics. Numerical simulations of both the quasi-incompressible model, intended for coastal waves simulations, and the compressible model, used for tsunami propagation, are presented in §5.

## 2. Derivation of the model

### *2.1. Governing equations and pressure distribution*

We study the propagation of waves in an inviscid compressible fluid with a density $\rho$ and a pressure $p$ in the case of a two-dimensional flow above an arbitrary bathymetry. The horizontal coordinate is $x$ (unit vector $\boldsymbol{e_x}$) and the vertical coordinate is $z$ (unit vector $\boldsymbol{e_z}$). The components of the fluid velocity field $\boldsymbol{v}$ are $u$ in the $Ox$-direction and $w$ in the $Oz$-direction. The bathymetry is measured by the elevation $b(x,t)$ of the bottom over a constant horizontal datum. Since the seabed can be displaced due to seismic effects, the bottom can be mobile and $b$ depends on $t$. The still water depth above the bottom is denoted by $h_0(x,t)$ and the total water depth by $h(x,t)$. The elevation of the free surface over the horizontal datum is $Z(x,t) = h(x,t) + b(x,t)$. The elevation of the free surface at rest over the horizontal datum is a constant $Z_0$ which can be chosen equal to zero (the horizontal datum is the still water level). In this case, $b = -h_0$ and $Z$ is equal to the wave elevation $\eta = h - h_0$. The notations are presented in figure 1. There is no particular smallness assumption on $b$ nor on its derivatives.

The continuity equation can be written

$$\frac{\partial \rho}{\partial t} + \frac{\partial \rho u}{\partial x} + \frac{\partial \rho w}{\partial z} = 0 \tag{1}$$

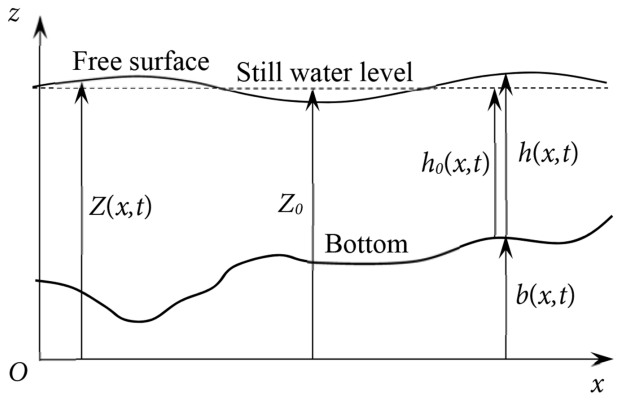


Figure 1: Definition sketch.

The vector of gravitational acceleration is denoted by $\boldsymbol{g} = -g\boldsymbol{e_z}$. The momentum balance equation in the $Ox$ and $Oz$-directions are respectively

$$\frac{\partial \rho u}{\partial t} + \frac{\partial \rho u^2}{\partial x} + \frac{\partial \rho uw}{\partial z} = -\frac{\partial p}{\partial x} \tag{2}$$

and

$$\frac{\partial \rho w}{\partial t} + \frac{\partial \rho uw}{\partial x} + \frac{\partial \rho w^2}{\partial z} = -\rho g - \frac{\partial p}{\partial z} \tag{3}$$

The boundary condition at the bottom reduces to the no-penetration condition

$$w(b) = \frac{\partial b}{\partial t} + u(b)\frac{\partial b}{\partial x} \tag{4}$$

The kinematic boundary condition at the free surface can be written

$$w(Z) = \frac{\partial Z}{\partial t} + u(Z)\frac{\partial Z}{\partial x} \tag{5}$$

The surface tension being neglected (this assumption restricts this study to waves with periods larger than about 0.1 s or wave lengths larger than a few centimetres), the dynamic boundary condition at the free surface states that the pressure at $z = Z$ is equal to the atmospheric pressure, which is supposed to be a constant that can be taken equal to zero. This leads to

$$p(Z) = 0 \tag{6}$$

Since the fluid is compressible, the mass and momentum equations are not sufficient to close the problem. The first law of thermodynamics and an equation of state must be added to describe completely the system. Previous works suggest that density stratification due to temperature or salinity variations have much smaller effects than the increase of ocean water density with depth due to the seawater compressibility in the gravity field (Tsai *et al.* 2013 [34], Watada 2013 [42]). Similarly, stratification effects due to temperature and salinity are neglected by Ardhuin & Herbers (2013) [43] in their study of noise excited by ocean

surface gravity waves. The fluid is likewise assumed to be barotropic by Renzi & Dias (2014) [44] for the propagation of hydro-acoustic waves generated by surface pressures disturbance in the ocean and by Kadri & Stiassnie (2013) [45] for acoustic-gravity waves. Note that bottom friction has a negligible effect in deep oceans, in particular on tsunami delay (Watada 2014 [39], Allgeyer & Cummins 2014 [35]).

The variation in sound velocity with depth would give a small correction to the effect of compressibility on wave propagation, which is already a small correction, even for a tsunami in deep ocean. It is thus wholly negligible. A depth-averaged model for hydro-acoustic waves generated by tsunamigenic ground motions was derived by Sammarco *et al.* (2013) [46] in a weakly compressible ocean. This model was later extended by Abdolali *et al.* (2015) [47] to include the effect of a compressible sediment layer. These hydro-acoustic waves are important as precursors of tsunamis and can be used for early warning systems. In these models too and also in the works cited above (Ardhuin & Herbers 2013 [43], Kadri & Stiassnie 2013 [45], Rensi & Dias 2014 [44]), the sound velocity was supposed to be constant in the ocean.

It follows that the following assumptions can be made: 1) The flow is homentropic i.e. the entropy $s$ is uniform and constant; 2) The fluid is barotropic; 3) The sound velocity, denoted by $a$, is uniform and constant. The same hypotheses were assumed by most authors. Consequently the equation of state is taken as

$$p = a^2 \left(\rho - \rho_s\right) \tag{7}$$

where $\rho_s$ is the seawater density at the free surface. It is of course also possible to write the well-known formula

$$\frac{\partial p}{\partial \rho} = a^2 \tag{8}$$

In the absence of waves, the ocean is supposed to be in hydrostatic equilibrium. The quantities evaluated in this state are denoted by a subscript 0. By definition the equilibrium hydrostatic pressure $p_0$ is related to the equilibrium density $\rho_0$ by

$$\frac{\partial p_0}{\partial z} = -\rho_0 g \tag{9}$$

In these conditions, the equation of state writes $p_0 = a^2(\rho_0 - \rho_s)$. The integration of (9) gives the basic hydrostatic ocean state (Abdolali & Kirby 2017 [37])

$$\rho_0 = \rho_s \mathrm{e}^{g(Z_0 - z)/a^2} \tag{10}$$

where $Z_0$ is the still water elevation. The expression of the pressure is then

$$p_0 = a^2 \rho_s \left[\mathrm{e}^{g(Z_0 - z)/a^2} - 1\right] \tag{11}$$

When a wave propagates in the ocean, this equilibrium hydrostatic state is perturbed. The perturbation can be divided into two effects: a hydrostatic perturbation due to the variation in water depth while the hydrostatic equation is still satisfied in the vertical direction (although not in the horizontal directions) and a non-hydrostatic effect induced by the vertical acceleration i.e. the left-hand side of (3). The pressure is thus written as the sum of a hydrostatic term $p_H$ and a non-hydrostatic term $p_N$ as

$$p = p_H + p_N \tag{12}$$

The hydrostatic term is the sum of the equilibrium hydrostatic state and a hydrostatic perturbation

$$p_H = p_0 + \delta p_H \tag{13}$$

The non-hydrostatic pressure corresponds to a density fluctuation $\rho_N$ such that $p_N = a^2 \rho_N$ and the hydrostatic pressure corresponds to a hydrostatic term $\rho_H$ in the density with

$$\rho = \rho_H + \rho_N \tag{14}$$

and $p_H = a^2(\rho_H - \rho_s)$. As explained in §2.2, the non-hydrostatic correction $p_N$ to the pressure and the corresponding density fluctuation $\rho_N$ are small in a shallow water flow. This implies that the leading contribution is hydrostatic.

By definition, the hydrostatic pressure is defined by

$$\frac{\partial p_H}{\partial z} = -\rho_H g \tag{15}$$

which gives

$$\rho_H = \rho_s \mathrm{e}^{g(Z-z)/a^2} \tag{16}$$

and

$$p_H = a^2 \rho_s \left[\mathrm{e}^{g(Z-z)/a^2} - 1\right] \tag{17}$$

Defining the water elevation by $\eta = Z - Z_0$, the hydrostatic density is related to its equilibrium value by the relation

$$\rho_H = \rho_0 \, \mathrm{e}^{g\eta/a^2} \tag{18}$$

Despite the term "static", the hydrostatic pressure $p_H$ depends on the time $t$ and on the abscissa $x$ in the presence of a wave, through the elevation $Z(x,t)$ of the free surface.

In the absence of heat transfer, the total energy conservation equation, expressed by the first law of thermodynamics, can be written

$$\frac{\partial}{\partial t}\left(\frac{1}{2}\rho v^2 + \rho g z + \rho e_i\right) + \mathrm{div}\left[\left(\frac{1}{2}\rho v^2 + \rho g z + \rho e_i + p\right)\boldsymbol{v}\right] = 0 \tag{19}$$

where $e_i$ is the specific internal energy. In the case of a homentropic flow (where the change in entropy $\mathrm{d}s = 0$),

the thermodynamic relation $\mathrm{d}e_i = T\mathrm{d}s + (p/\rho^2)\mathrm{d}\rho$ (with $T$ being the temperature) reduces to

$$\mathrm{d}e_i = \frac{p}{\rho^2}\mathrm{d}\rho \tag{20}$$

Since the non-hydrostatic contribution is small, the main contribution to the internal energy is hydrostatic and can be explicitly expressed. Denoted by $e_{iH}$, this part of the internal energy can be found with relation (20) and the state equation (7) as

$$\frac{\mathrm{d}e_{iH}}{\mathrm{d}\rho_H} = a^2\frac{\rho_H - \rho_s}{\rho_H^2} \tag{21}$$

The integration of this equation together with the expression of $\rho_H$ (16) gives the expression of $E_{iH} = \rho_H e_{iH}$

$$E_{iH} = \rho_H g(Z - z) - p_H \tag{22}$$

The total internal energy is the sum of this leading hydrostatic contribution and a non-hydrostatic correction.

### *2.2. Scaling and dimensionless equations*

The model is derived under the assumption of a shallow water flow, which is valid even for a tsunami in a deep ocean. Denoting a characteristic depth by $h_0$ and a characteristic length by $L$ of the flow in the $Ox$-direction, the problem admits a a small parameter

$$\varepsilon = \frac{h_0}{L} \ll 1 \tag{23}$$

Since the bathymetry is arbitrary, the characteristic variation length of $b$ in the $Ox$-direction is the characteristic length $L$ of the flow.

The model is derived with an asymptotic method. The equations are thus written in a dimensionless form to evaluate the order of magnitude of each term with respect to the small parameter $\varepsilon$.

Denoting by $u_0$ a characteristic horizontal fluid velocity, the Froude number is defined as $F = u_0/\sqrt{gh_0}$. For a tsunami in deep oceans, $F$ can be very small. However no assumption is made on the order of magnitude of $F$ (i.e. $F = O[1]$) in order to derive a general model, including coastal waves. Besides, the case $F = O(1)$ covers the particular cases where $F$ is small whereas the converse is not true. In the following, $F$ is taken equal to 1 to lighten the equations (i.e. the characteristic velocity $u_0$ is taken equal to $\sqrt{gh_0}$) with no loss of generality because the final equations in dimensional form are the same.

The following scaling for $x$, $z$, $h$, $t$, $u$, $w$ is classical in the shallow water context (a tilde denotes a dimensionless quantity):

$$\tilde{x} = \frac{x}{L}\ ;\quad \tilde{z} = \frac{z}{h_0}\ ;\quad \tilde{h} = \frac{h}{h_0}\ ;\quad \tilde{t} = t\frac{\sqrt{gh_0}}{L}$$
$$\tilde{u} = \frac{u}{\sqrt{gh_0}}\ ;\quad \tilde{w} = \frac{w}{\varepsilon\sqrt{gh_0}}\ ; \tag{24}$$

We write also $\tilde{b} = b/h_0$ and $\tilde{Z} = Z/h_0$.

The usual Mach number is $Ma = u_0/a$ but, for convenience, the Mach number is defined with the incompressible surface waves celerity as

$$M = \frac{\sqrt{gh}}{a} \tag{25}$$

The Mach number in the reference state is $M_0 = \sqrt{gh_0}/a$. The relations between these numbers in the reference state is $M_0 = Ma/F$. The order of magnitude of $M_0$ is estimated with respect to $\varepsilon$. Even if compressibility is taken into account in this model, the fluids considered here are weakly compressible and therefore the Mach number is small. As there is no reason for the Mach number to be an integer power of $\varepsilon$, it is written

$$M_0 = \varepsilon^\gamma M_1 \tag{26}$$

where $0 < \gamma \leqslant 1$ and $M_1 = O(1)$. In practice, only the square of the Mach number occurs in the equations. Since $M_0^2 = O(\varepsilon^{2\gamma})$ with $0 < 2\gamma \leqslant 2$, if an integer power of $\varepsilon$ is absolutely required, it is possible to choose $\gamma = 1/2$ and thus $M_0^2 = O(\varepsilon)$ or $\gamma = 1$ and $M_0^2 = O(\varepsilon^2)$. The main consequence of assumption (26) with $0 < \gamma \leqslant 1$ is that the non-hydrostatic contribution $\rho_N$ to density fluctuation is negligible unlike the hydrostatic contribution $\rho_H$.

Shear effects, due to the variation on horizontal fluid velocity with depth, can be important nearshore, especially in the case of breaking, but in the deep ocean where compressibility can have a measurable effect, they are negligible. Although it is straightforward to include shear (see Kazakova & Richard, 2019 [48]), shear is not important in the present study and so is omitted to simplify the equations. Therefore the order of magnitude of shear effects will be chosen so that they are neglected consistently in the equations. Denoting by $U$ the depth-averaged horizontal velocity and $u' = u - U$ the deviation of the horizontal velocity with respect to this average value, $u'$ is supposed to be small and to scale with $\varepsilon^\beta\sqrt{gh_0}$ such that $\tilde{u} = \tilde{U} + \varepsilon^\beta\tilde{u}'$ with $\beta > 1$. This approach is due to Teshukov (2007) [49] who considered the case $0 < \beta < 1$ to include explicitly shear effects but not dispersive terms, whereas $\beta$ is here greater than 1 to neglect shear terms while including dispersive terms. This approach can be also related to the vorticity. If the vorticity $\omega = \partial u/\partial z - \partial w/\partial x$ is of $O(\varepsilon^\alpha)$, then $\beta = \min(\alpha, 2)$ since, defining $\varepsilon^\alpha\tilde{\omega} = \omega\sqrt{h_0/g}$, we have $\varepsilon^\alpha\tilde{\omega} = \varepsilon^\beta\partial\tilde{u}'/\partial\tilde{z} - \varepsilon^2\partial\tilde{w}/\partial\tilde{x}$. In the irrotational case, which is a common assumption for non-breaking waves or for tsunami propagation in deep ocean, $\beta = 2$.

The pressure and density are scaled as in the incompressible case, with the surface density $\rho_s$ as reference density,

$$\tilde{\rho} = \frac{\rho}{\rho_s}\ ;\quad \tilde{p} = \frac{p}{\rho_s g h_0} \tag{27}$$

The dimensionless mass and momentum balance equations in the $Ox$ and $Oz$ directions become respectively

$$\frac{\partial\tilde{\rho}}{\partial\tilde{t}} + \frac{\partial\tilde{\rho}\tilde{u}}{\partial\tilde{x}} + \frac{\partial\tilde{\rho}\tilde{w}}{\partial\tilde{z}} = 0 \tag{28}$$

$$\frac{\partial \tilde{\rho}\tilde{u}}{\partial \tilde{t}} + \frac{\partial \tilde{\rho}\tilde{u}^2}{\partial \tilde{x}} + \frac{\partial \tilde{\rho}\tilde{u}\tilde{w}}{\partial \tilde{z}} = -\frac{\partial \tilde{p}}{\partial \tilde{x}} \tag{29}$$

and

$$\varepsilon^2 \left( \frac{\partial \tilde{\rho}\tilde{w}}{\partial \tilde{t}} + \frac{\partial \tilde{\rho}\tilde{u}\tilde{w}}{\partial \tilde{x}} + \frac{\partial \tilde{\rho}\tilde{w}^2}{\partial \tilde{z}} \right) = -\tilde{\rho} - \frac{\partial \tilde{p}}{\partial \tilde{z}} \tag{30}$$

Taking into account the definition of the hydrostatic pressure (15), the last equation can be reduced to

$$\varepsilon^2 \left( \frac{\partial \tilde{\rho}\tilde{w}}{\partial \tilde{t}} + \frac{\partial \tilde{\rho}\tilde{u}\tilde{w}}{\partial \tilde{x}} + \frac{\partial \tilde{\rho}\tilde{w}^2}{\partial \tilde{z}} \right) = -\tilde{\rho}_N - \frac{\partial \tilde{p}_N}{\partial \tilde{z}} \tag{31}$$

which shows that $p_N = O(\varepsilon^2)$. The dimensionless non-hydrostatic pressure is thus redefined as

$$\tilde{p}_N = \frac{p_N}{\varepsilon^2 \rho_s g h_0} \tag{32}$$

This gives the relation $\tilde{p} = \tilde{p}_H + \varepsilon^2 \tilde{p}_N$, showing that the non-hydrostatic pressure is a small correction to the pressure. From $p_N = a^2 \rho_N$ we deduce that

$$\tilde{\rho}_N = \varepsilon^{2+2\gamma} M_1^2 \tilde{p}_N \tag{33}$$

which implies that the perturbation to the density due to the non-hydrostatic pressure is very small (of $O[\varepsilon^3]$ if $\gamma = 1/2$ or of $O[\varepsilon^4]$ if $\gamma = 1$) and negligible in front of the hydrostatic part of the density. The definition of $\tilde{\rho}_N$ is thus changed into

$$\tilde{\rho}_N = \frac{\rho_N}{\varepsilon^{2+2\gamma} \rho_s} \tag{34}$$

and $\tilde{\rho}_N = M_1^2 \tilde{p}_N$. This means that $\tilde{\rho} = \tilde{\rho}_H + O(\varepsilon^{2+2\gamma})$.

In the incompressible limit, $p_N$ is also of $O(\varepsilon^2)$ with $\rho_N = 0$, which is possible given that $a \to \infty$ (or $M_0 = 0$). In the weakly compressible approach, the non-hydrostatic pressure retains the same order of magnitude with a large but finite sound velocity (or a small but non-zero Mach number) and a very small density perturbation.

With the new scaling for $p_N$ and $\rho_N$, the equation (31) becomes

$$\frac{\partial \tilde{\rho}\tilde{w}}{\partial \tilde{t}} + \frac{\partial \tilde{\rho}\tilde{u}\tilde{w}}{\partial \tilde{x}} + \frac{\partial \tilde{\rho}\tilde{w}^2}{\partial \tilde{z}} = -\varepsilon^{2\gamma} \tilde{\rho}_N - \frac{\partial \tilde{p}_N}{\partial \tilde{z}} \tag{35}$$

The corrective term on the weight due to the non-hydrostatic effect is thus small and it can be consistently ignored given that all other terms are already of $O(\varepsilon^2)$, writing

$$\frac{\partial \tilde{\rho}\tilde{w}}{\partial \tilde{t}} + \frac{\partial \tilde{\rho}\tilde{u}\tilde{w}}{\partial \tilde{x}} + \frac{\partial \tilde{\rho}\tilde{w}^2}{\partial \tilde{z}} = -\frac{\partial \tilde{p}_N}{\partial \tilde{z}} + O\left(\varepsilon^{2\gamma}\right) \tag{36}$$

The dimensionless form of the equation of state restricted to the leading hydrostatic part of the pressure is

$$\tilde{p}_H = \frac{\tilde{\rho}_H - 1}{\varepsilon^{2\gamma} M_1^2} \tag{37}$$

This implies that $\tilde{\rho}_H = 1 + O(\varepsilon^{2\gamma})$. The weak compressibility implies that the density differs only slightly from its surface value $\rho_s$. However this difference is not negligible since the dispersive non-hydrostatic terms which are taken into account are of $O(\varepsilon^2)$. This difference $\rho'$ is defined as $\rho_H = \rho_s + \rho'$ and scaled as $\tilde{\rho}' = \rho'/(\varepsilon^{2\gamma}\rho_s)$. In dimensionless form, we have

$$\tilde{\rho}_H = 1 + \varepsilon^{2\gamma} \tilde{\rho}' \tag{38}$$

It follows that the mass conservation equation (28) can be written

$$\frac{\partial \tilde{u}}{\partial \tilde{x}} + \frac{\partial \tilde{w}}{\partial \tilde{z}} + \varepsilon^{2\gamma} \left( \frac{\partial \tilde{\rho}'}{\partial \tilde{t}} + \frac{\partial \tilde{\rho}'\tilde{u}}{\partial \tilde{x}} + \frac{\partial \tilde{\rho}'\tilde{w}}{\partial \tilde{z}} \right) = O\left(\varepsilon^{2+2\gamma}\right) \tag{39}$$

The first two terms are the leading incompressible terms. The following terms of $O(\varepsilon^{2\gamma})$ are the compressible hydrostatic correction and the right-hand side of $O(\varepsilon^{2+2\gamma})$ is the neglected compressible non-hydrostatic correction. In the same way, the horizontal momentum balance equation writes

$$\frac{\partial \tilde{\rho}_H \tilde{u}}{\partial \tilde{t}} + \frac{\partial \tilde{\rho}_H \tilde{u}^2}{\partial \tilde{x}} + \frac{\partial \tilde{\rho}_H \tilde{u}\tilde{w}}{\partial \tilde{z}} + \frac{\partial \tilde{p}_H}{\partial \tilde{x}} + \varepsilon^2 \frac{\partial \tilde{p}_N}{\partial \tilde{x}} = O\left(\varepsilon^{2+2\gamma}\right) \tag{40}$$

where the hydrostatic perturbation $\tilde{\rho}'$ is included in $\tilde{\rho}_H$, giving terms of $O(\varepsilon^{2\gamma})$.

### *2.3. Depth-averaged equations*

#### *2.3.1. Depth-averaged quantity*

The governing equations are averaged over the depth. For any quantity $A$, its depth-averaged value for a compressible fluid can be defined in two ways. The first average, denoted by $\langle A \rangle$, is the depth-average counterpart of the Favre averaging and is defined as

$$\langle A \rangle = \frac{\displaystyle\int_b^Z \rho A \, \mathrm{d}z}{\displaystyle\int_b^Z \rho \, \mathrm{d}z} \tag{41}$$

The second average is denoted by $\overline{A}$ and is the usual depth average

$$\overline{A} = \frac{1}{h} \int_b^Z A \, \mathrm{d}z \tag{42}$$

Since $\rho = \rho_H + \varepsilon^{2+2\gamma} \rho_N$, the first average can be written

$$\langle A \rangle = \frac{\displaystyle\int_b^Z \rho_H A \, \mathrm{d}z}{\displaystyle\int_b^Z \rho_H \, \mathrm{d}z} + O\left(\varepsilon^{2+2\gamma}\right) \tag{43}$$

Introducing the normalized depth-averaged hydrostatic density $R = \overline{\rho_H}/\rho_s$ leads to the following relations in dimensional and dimensionless forms

$$\int_b^Z \rho_H A \, \mathrm{d}z = \rho_s h R \langle A \rangle \;\; ; \quad \int_{\tilde{b}}^{\tilde{Z}} \tilde{\rho}_H \tilde{A} \, \mathrm{d}\tilde{z} = \tilde{h} R \langle \tilde{A} \rangle \tag{44}$$

The following notations are used for the average fluid horizontal velocity, for the average fluid vertical velocity (both being of the Favre type) and for the normalized average non-hydrostatic pressure: $U = \langle u \rangle$, $W = \langle w \rangle$ and $P = \overline{p_N}/\rho_s$ (which gives $\tilde{P} = \overline{\tilde{p}_N}$ in dimensionless form with $P = \varepsilon^2 g h_0 \tilde{P}$). From the definition $u = U + u'$, it follows that $\langle u' \rangle = 0$. This implies also that $\overline{\tilde{u}} = \tilde{U} + O(\varepsilon^{\beta+2\gamma})$. In the case of the horizontal fluid velocity, the difference between the two averages is negligible if $\gamma > 1/2$ or if $\beta = 2$ (irrotational flow). In the case of the fluid vertical velocity, $\tilde{W} = \overline{\tilde{w}} + O(\varepsilon^{2\gamma})$.

An expression for the average density $R$ can be found from the integration of (16) which yields

$$R = \frac{\mathrm{e}^{M^2} - 1}{M^2} \tag{45}$$

Since the Mach number is small, the development of this expression can be restricted to

$$R = 1 + \frac{M^2}{2} + O(M^4) \tag{46}$$

*2.3.2. Mass conservation*

With the above definitions, and taking into account the kinematic boundary condition, the integration of the mass conservation equation over the fluid depth gives

$$\frac{\partial \tilde{h} R}{\partial \tilde{t}} + \frac{\partial \tilde{h} \tilde{U} R}{\partial \tilde{x}} = O(\varepsilon^{2+2\gamma}) \tag{47}$$

This equation can be written

$$\left( R + \tilde{h} \frac{\mathrm{d}R}{\mathrm{d}\tilde{h}} \right) \left( \frac{\partial \tilde{h}}{\partial \tilde{t}} + \frac{\partial \tilde{h} \tilde{U}}{\partial \tilde{x}} \right) - h^2 \frac{\mathrm{d}R}{\mathrm{d}\tilde{h}} \frac{\partial \tilde{U}}{\partial \tilde{x}} = O(\varepsilon^{2+2\gamma}) \tag{48}$$

The expression (45) of $R$ yields $R + \tilde{h}\mathrm{d}R/\mathrm{d}\tilde{h} = \mathrm{e}^{M^2}$ which leads to

$$\frac{\partial \tilde{h}}{\partial \tilde{t}} + \frac{\partial \tilde{h} \tilde{U}}{\partial \tilde{x}} = \frac{M^2}{2} Q_0 \tilde{h} \frac{\partial \tilde{U}}{\partial \tilde{x}} + O(\varepsilon^{2+2\gamma}) \tag{49}$$

where

$$Q_0 = \frac{2}{M^4} \left( \mathrm{e}^{-M^2} + M^2 - 1 \right) \tag{50}$$

The expression of $Q_0$ can also be written

$$Q_0 = 1 - \frac{M^2}{3} + O(M^4) \tag{51}$$

The fluid compressibility implies that the right-hand side of (49) is not zero. However the mass conservation equation is expressed by (47). Note that the exact depth-averaged mass conservation equation is

$$\frac{\partial h \overline{\rho}}{\partial t} + \frac{\partial h \overline{\rho} U}{\partial x} = 0 \tag{52}$$

and $\tilde{\overline{\rho}} = R + O(\varepsilon^{2+2\gamma})$.

*2.3.3. Momentum balance equation*

The integration of the momentum balance equation (40) in the horizontal direction, taking into account the boundary conditions, leads to

$$\frac{\partial \tilde{h} R \tilde{U}}{\partial \tilde{t}} + \frac{\partial}{\partial \tilde{x}} \left( \tilde{h} R \langle \tilde{u}^2 \rangle + \int_{\tilde{b}}^{\tilde{Z}} \tilde{p}_H \, \mathrm{d}\tilde{z} + \varepsilon^2 \tilde{h} \tilde{P} \right) = -\tilde{p}(b) \frac{\partial \tilde{b}}{\partial \tilde{x}} + O(\varepsilon^{2+2\gamma}) \tag{53}$$

The definition of $u'$ enables to write $\langle \tilde{u}^2 \rangle = \tilde{U}^2 + \varepsilon^{2\beta} \langle u'^2 \rangle$. Since $2\beta > 2$, the $O(\varepsilon^{2\beta})$ term is negligible. The integral of the hydrostatic pressure can be calculated with the expression (17) which becomes in dimensionless form $M_0^2 \tilde{p}_H = \exp[M_0^2(\tilde{Z} - \tilde{z})] - 1$ and which gives $\tilde{p}_H(b) = \tilde{h} R$. The depth-integrated horizontal momentum balance equation can be written

$$\frac{\partial \tilde{h} R \tilde{U}}{\partial \tilde{t}} + \frac{\partial}{\partial \tilde{x}} \left( \tilde{h} R \tilde{U}^2 + Q_1 \frac{\tilde{h}^2}{2} + \varepsilon^2 \tilde{h} \tilde{P} \right) = -\tilde{h} R \frac{\partial \tilde{b}}{\partial \tilde{x}} - \varepsilon^2 \tilde{p}_N(b) \frac{\partial \tilde{b}}{\partial \tilde{x}} + O(\varepsilon^{2\beta}) + O(\varepsilon^{2+2\gamma}) \tag{54}$$

where

$$Q_1 = \frac{2}{M^4} \left( \mathrm{e}^{M^2} - M^2 - 1 \right) \tag{55}$$

which can be written

$$Q_1 = 1 + \frac{M^2}{3} + O(M^4) \tag{56}$$

In the vertical direction, integration over the depth of (36) with the boundary conditions gives

$$\frac{\partial \tilde{h} R \tilde{W}}{\partial \tilde{t}} + \frac{\partial \tilde{h} R \langle \tilde{u} \tilde{w} \rangle}{\partial \tilde{x}} = \tilde{p}_N(b) + O(\varepsilon^{2\gamma}) \tag{57}$$

Since $\tilde{u} = \tilde{U} + \varepsilon^\beta \tilde{u}'$, we can write $\langle \tilde{u} \tilde{w} \rangle = \tilde{U} \tilde{W} + O(\varepsilon^\beta)$. Asymptotic expressions of $p_N$ are needed to evaluate the non-hydrostatic pressure at the bottom $\tilde{p}_N(b)$ in (54) and (57).

Firstly, an asymptotic expression of the vertical velocity is obtained from the mass conservation equation (39) and from the decomposition $\tilde{u} = \tilde{U} + \varepsilon^\beta \tilde{u}'$:

$$\frac{\partial \tilde{w}}{\partial \tilde{z}} = -\frac{\partial \tilde{U}}{\partial \tilde{x}} + O(\varepsilon^\beta) + O(\varepsilon^{2\gamma}) \tag{58}$$

Integration of this relation with the no-penetration boundary condition shows that the variation of the vertical velocity in the depth is linear at this level of approximation. This gives

$$\tilde{w} = (\tilde{b} - \tilde{z}) \frac{\partial \tilde{U}}{\partial \tilde{x}} + \frac{\partial \tilde{b}}{\partial \tilde{t}} + \tilde{U} \frac{\partial \tilde{b}}{\partial \tilde{x}} + O(\varepsilon^\beta) + O(\varepsilon^{2\gamma}) \tag{59}$$

with the depth-averaged vertical velocity

$$\tilde{W} = -\frac{\tilde{h}}{2} \frac{\partial \tilde{U}}{\partial \tilde{x}} + \frac{\partial \tilde{b}}{\partial \tilde{t}} + \tilde{U} \frac{\partial \tilde{b}}{\partial \tilde{x}} + O(\varepsilon^\beta) + O(\varepsilon^{2\gamma}) \tag{60}$$

Secondly the non-hydrostatic pressure is obtained by integration of the momentum balance equation in the vertical direction (36) which can be also consistently written

$$\frac{\partial \tilde{p}_N}{\partial \tilde{z}} = -\left(\frac{\partial \tilde{w}}{\partial \tilde{t}} + \frac{\partial \tilde{U}\tilde{w}}{\partial \tilde{x}} + \frac{\partial \tilde{w}^2}{\partial \tilde{z}}\right) + O(\varepsilon^{\beta}) + O(\varepsilon^{2\gamma}) \quad (61)$$

In this expression $\tilde{w}$ is replaced by the linear asymptotic law (59). The obtained relation is integrated from the free surface to an altitude $z$. At the free surface, $z = Z$ and the dynamic boundary condition gives $p_N(Z) = 0$. It follows that the non-hydrostatic pressure profile in the depth is parabolic with

$$\tilde{p}_N = \left[\frac{\tilde{Z}^2 - \tilde{z^2}}{2} - \tilde{b}\left(\tilde{Z} - \tilde{z}\right)\right]\left[2\left(\frac{\partial \tilde{U}}{\partial \tilde{x}}\right)^2 - \frac{\partial^2 \tilde{U}}{\partial \tilde{x}\partial \tilde{t}} - \frac{\partial}{\partial \tilde{x}}\left(\tilde{U}\frac{\partial \tilde{U}}{\partial \tilde{x}}\right)\right] + \left(\tilde{Z} - \tilde{z}\right)\ddot{\tilde{b}} + O(\varepsilon^{\beta}) + O(\varepsilon^{2\gamma}) \quad (62)$$

where the material derivative is defined as

$$\dot{b} = \frac{\mathrm{D}b}{\mathrm{D}t} = \frac{\partial b}{\partial t} + U\frac{\partial b}{\partial x}\,; \quad \ddot{b} = \frac{\mathrm{D}\dot{b}}{\mathrm{D}t} \quad (63)$$

The consistent expression of the non-hydrostatic pressure at the bottom is thus

$$\tilde{p}_N(b) = -\frac{\tilde{h}^2}{2}\left[\frac{\partial^2 \tilde{U}}{\partial \tilde{x}\partial \tilde{t}} + \tilde{U}\frac{\partial^2 \tilde{U}}{\partial \tilde{x}^2} - \left(\frac{\partial \tilde{U}}{\partial \tilde{x}}\right)^2\right] + \tilde{h}\ddot{\tilde{b}} + O(\varepsilon^{\beta}) + O(\varepsilon^{2\gamma}) \quad (64)$$

Taking the usual depth average of (62) gives the average non-hydrostatic pressure $\tilde{P} = \overline{\tilde{p}_N}$

$$\tilde{P} = -\frac{\tilde{h}^2}{3}\left[\frac{\partial^2 \tilde{U}}{\partial \tilde{x}\partial \tilde{t}} + \tilde{U}\frac{\partial^2 \tilde{U}}{\partial \tilde{x}^2} - \left(\frac{\partial \tilde{U}}{\partial \tilde{x}}\right)^2\right] + \frac{\tilde{h}}{2}\ddot{\tilde{b}} + O(\varepsilon^{\beta}) + O(\varepsilon^{2\gamma}) \quad (65)$$

This implies that the non-hydrostatic pressure at the bottom can be consistently written

$$\tilde{p}_N(b) = \frac{3}{2}\tilde{P} + \frac{\tilde{h}}{4}\ddot{\tilde{b}} + O(\varepsilon^{\beta}) + O(\varepsilon^{2\gamma}) \quad (66)$$

This expression is used in (57). Consequently, using again $R = 1 + O(\varepsilon^{2\gamma})$, the depth-integrated vertical momentum balance equation is

$$\frac{\partial \tilde{h}R\tilde{W}}{\partial \tilde{t}} + \frac{\partial \tilde{h}R\tilde{U}\tilde{W}}{\partial \tilde{x}} = \frac{3}{2}\tilde{P} + \frac{\tilde{h}R}{4}\ddot{\tilde{b}} + O(\varepsilon^{\beta}) + O(\varepsilon^{2\gamma}) \quad (67)$$

This can be rewritten as

$$\frac{\partial \tilde{h}R\tilde{\mathcal{W}}}{\partial \tilde{t}} + \frac{\partial \tilde{h}R\tilde{U}\tilde{\mathcal{W}}}{\partial \tilde{x}} = \frac{3}{2}\tilde{P} + O(\varepsilon^{\beta}) + O(\varepsilon^{2\gamma}) \quad (68)$$

where $\mathcal{W}$ is a modified average vertical velocity defined by

$$\mathcal{W} = W - \frac{\dot{b}}{4} \quad (69)$$

Another way to express consistently the non-hydrostatic pressure at the bottom is

$$\tilde{p}_N(b) = 2\tilde{P} + \frac{\tilde{h}}{3}\frac{\mathrm{D}}{\mathrm{D}\tilde{t}}\left(\frac{\mathrm{D}\tilde{b}}{\mathrm{D}\tilde{t}} - \tilde{W}\right) + O(\varepsilon^{2\gamma}) + O(\varepsilon^{\beta}) \quad (70)$$

When used in (54) this gives

$$\frac{\partial \tilde{h}R\tilde{U}}{\partial \tilde{t}} + \frac{\partial}{\partial \tilde{x}}\left(\tilde{h}R\tilde{U}^2 + Q_1\frac{\tilde{h}^2}{2} + \varepsilon^2\tilde{h}\tilde{P}\right) = -\left(\tilde{h}R + \varepsilon^2 2\tilde{P}\right)\frac{\partial \tilde{b}}{\partial \tilde{x}} + \varepsilon^2\frac{\tilde{h}R}{3}\frac{\partial \tilde{b}}{\partial \tilde{x}}\frac{\mathrm{D}}{\mathrm{D}\tilde{t}}\left(\tilde{W} - \dot{\tilde{b}}\right) + O(\varepsilon^{2+2\gamma}) + O(\varepsilon^{2\beta}) \quad (71)$$

This equation is useful to prove the conservation of energy. However an equivalent form of this equation is derived for convenience. Given that $R = 1 + O(\varepsilon^{2\gamma})$, the expression (70) is equivalent to (66) since it is possible to write

$$\tilde{p}_N(b) = 2\tilde{P} + \frac{\tilde{h}R}{3}\frac{\mathrm{D}}{\mathrm{D}\tilde{t}}\left(\frac{\mathrm{D}\tilde{b}}{\mathrm{D}\tilde{t}} - \tilde{W}\right) + O(\varepsilon^{2\gamma}) + O(\varepsilon^{\beta}) \quad (72)$$

Using (67), $\tilde{h}R\mathrm{D}\tilde{W}/\mathrm{D}\tilde{t}$ can be replaced in the above expression leading to

$$\tilde{p}_N(b) = \frac{3}{2}\tilde{P} + \frac{\tilde{h}R}{4}\ddot{\tilde{b}} + O(\varepsilon^{\beta}) + O(\varepsilon^{2\gamma}) \quad (73)$$

which is used in (67). This leads to the depth-averaged momentum balance equation in the $Ox$-direction which can be written

$$\frac{\partial \tilde{h}R\tilde{\mathcal{U}}}{\partial \tilde{t}} + \frac{\partial}{\partial \tilde{x}}\left(\tilde{h}R\tilde{U}\tilde{\mathcal{U}} + Q_1\frac{\tilde{h}^2}{2} + \varepsilon^2\tilde{h}\tilde{P}\right) = -\left(\tilde{h}R + \varepsilon^2\frac{3}{2}\tilde{P}\right)\frac{\partial \tilde{b}}{\partial \tilde{x}} + \varepsilon^2\tilde{h}R\frac{\dot{\tilde{b}}}{4}\frac{\mathrm{D}}{\mathrm{D}\tilde{t}}\left(\frac{\partial \tilde{b}}{\partial \tilde{x}}\right) + O(\varepsilon^{2+2\gamma}) + O(\varepsilon^{2\beta}) \quad (74)$$

where $\mathcal{U}$ is a modified average horizontal velocity defined by

$$\mathcal{U} = U + \frac{\dot{b}}{4}\frac{\partial b}{\partial x} \quad (75)$$

With the new variables $\mathcal{U}$ and $\mathcal{W}$, the hyperbolic system of equations has no more equations in the case of an arbitrary bathymetry than in the case of constant depth where $\mathcal{U}$ and $\mathcal{W}$ reduce to $U$ and $W$ respectively.

*2.3.4. Energy equation and non-hydrostatic pressure equation*

So far four variables have been introduced to describe the depth-averaged flow: $h$, $U$ (or $\mathcal{U}$), $W$ (or $\mathcal{W}$), and $P$. The average density $R$ is not an independent variable since it is a function of $h$. Only three equations have been derived: (47), (74) and (68). Equation (49) is equivalent to (47). An evolution equation for $P$ is needed to close the system in order to obtain a hyperbolic system (use of equation (60) or (65) would lead to a non-hyperbolic system).

The energy conservation equation (19) is integrated over the depth. Since $\tilde{\rho} = \tilde{\rho}_H + O(\varepsilon^{2+2\gamma})$ (see §2.2), the potential energy reduces to its hydrostatic part $\rho_H g z$. The integral of the sum of the hydrostatic part of the internal energy and of the potential energy is then

$$\frac{1}{\rho_s}\int_b^Z (E_{iH} + \rho_H g z)\,\mathrm{d}z = Q_2\frac{gh^2}{2} + ghRb \tag{76}$$

where

$$Q_2 = \frac{2}{M^4}\left[1 + \left(M^2-1\right)\mathrm{e}^{M^2}\right] = 1 + \frac{2M^2}{3} + O(M^4) \tag{77}$$

In the flux of (19), the quantity $E_{iH} + \rho_H g z + p_H$ is equal to $\rho_H g Z$. It follows that, to integrate over the depth the energy equation (19), we have to calculate the integral

$$\int_b^Z \rho_H g Z u\,\mathrm{d}z = gZU\int_b^Z \rho_H\,\mathrm{d}z + gh\int_b^Z \rho_H u'\,\mathrm{d}z \tag{78}$$

taking into account the decomposition $u = U + u'$. In the right-hand side of this equation, the first integral is equal to $hR$ and the second integral is equal to zero since by definition $\langle u'\rangle = 0$.

Consequently the integral of the energy equation (19) can be written

$$\begin{aligned}\frac{\partial}{\partial t}&\left(hR\frac{\langle u^2\rangle}{2} + hR\frac{\langle w^2\rangle}{2} + Q_2\frac{gh^2}{2} + ghRb + hRe_{\mathrm{int}}\right)\\ &+ \frac{\partial}{\partial x}\left[hR\frac{\langle u^3\rangle}{2} + hR\frac{\langle uw^2\rangle}{2} + hRUe_{\mathrm{int}}\right.\\ &\qquad\left. + gh^2RU + ghRbU + hUP\right] = p(b)\frac{\partial b}{\partial t}\end{aligned} \tag{79}$$

where $e_{\mathrm{int}}$ is a non-hydrostatic contribution to the energy, which plays the role of an internal energy for the model. Neglecting terms of $O(\varepsilon^{2\beta})$, we can write $\langle u^2\rangle \simeq U^2$ and $\langle u^3\rangle \simeq U^3$. The term $\langle uw^2\rangle$ corresponds to terms of $O(\varepsilon^2)$ in the momentum balance equations. It is thus consistent to neglect the correction of $O(\varepsilon^\beta)$ writing $\langle uw^2\rangle \simeq U\langle w^2\rangle$. Decomposing the vertical velocity as $w = W + w'$ leads to $\langle w^2\rangle = W^2 + \langle w'^2\rangle$ since by definition $\langle w'\rangle = 0$. With the expressions (59) and (60) of $w$ and $W$, it is easy to calculate that

$$\langle w'^2\rangle = \frac{\left(W - \dot{b}\right)^2}{3} \tag{80}$$

In the energy, the potential energy is $Q_2 gh^2/2 + ghRb$. The term $ghRb$ is included in the potential energy since the average elevation of the flow over the horizontal datum is $b + h/2$. However the non-uniformity of the density due to compressibility is responsible for the factor $Q_2$.

In the momentum balance equation (74), the term

$$\Pi = Q_1\frac{gh^2}{2} + hP \tag{81}$$

plays the role of a pressure (by analogy with the Euler equations of compressible fluids). Noticing that $Q_1 + Q_2 = 2R$, the energy conservation equation can be written

$$\frac{\partial hRe}{\partial t} + \frac{\partial}{\partial x}\left(hRUe + \Pi U\right) = \mathcal{P}_{\mathrm{ext}} \tag{82}$$

where the total energy is

$$e = \frac{U^2}{2} + \frac{W^2}{2} + \frac{\left(W - \dot{b}\right)^2}{6} + \frac{Q_2}{R}\frac{gh}{2} + gb + e_{\mathrm{int}} \tag{83}$$

and where $\mathcal{P}_{\mathrm{ext}} = p(b)\partial b/\partial t$ is the power introduced by the external forces. Due to the mobile bottom, the total energy of the system is not conserved because the external forces do work. The external power is

$$\mathcal{P}_{\mathrm{ext}} = ghR\frac{\partial b}{\partial t} + \left[2P + \frac{hR}{3}\frac{\mathrm{D}}{\mathrm{D}t}\left(\dot{b} - W\right)\right]\frac{\partial b}{\partial t} \tag{84}$$

This power is equal to zero if the bottom is not mobile i.e. if $\partial b/\partial t = 0$. In the expression, the first term is due to the hydrostatic pressure and the second term is due to the non-hydrostatic pressure, in both cases evaluated at the bottom ($z = b$).

From the depth-averaged mass and momentum equations (47), (71) and (67), it is possible to derive a balance equation for the mechanical energy of the model. Equation (71) can be written in dimensional form as

$$\begin{aligned}\frac{\partial hRU}{\partial t} + \frac{\partial}{\partial x}&\left(hRU^2 + Q_1\frac{gh^2}{2} + hP\right)\\ &= -\left(ghR + 2P\right)\frac{\partial b}{\partial x} + \frac{hR}{3}\frac{\partial b}{\partial x}\frac{\mathrm{D}}{\mathrm{D}t}\left(W - \dot{b}\right)\end{aligned} \tag{85}$$

while the dimensional form of (67) is simply

$$\frac{\partial hRW}{\partial t} + \frac{\partial hRUW}{\partial x} = \frac{3}{2}P + \frac{hR}{4}\ddot{b} \tag{86}$$

Taking into account the mass conservation equation (47), equations (85) and (67) can be written respectively as

$$\begin{aligned}hR&\left(\frac{\partial U}{\partial t} + U\frac{\partial U}{\partial x}\right) + \frac{\partial}{\partial x}\left(Q_1\frac{gh^2}{2} + hP\right)\\ &= -\left(ghR + 2P\right)\frac{\partial b}{\partial x} + \frac{hR}{3}\frac{\partial b}{\partial x}\frac{\mathrm{D}}{\mathrm{D}t}\left(W - \dot{b}\right)\end{aligned} \tag{87}$$

and

$$hR\left(\frac{\partial W}{\partial t} + U\frac{\partial W}{\partial x}\right) = \frac{3}{2}P + \frac{hR}{4}\ddot{b} \tag{88}$$

Forming

$$\frac{1}{2}\left[U\times(85)+U\times(87)\right]+\frac{2}{3}\left[W\times(86)+W\times(88)\right] \quad (89)$$

and noticing that

$$U\frac{\partial}{\partial x}\left(Q_1\frac{gh^2}{2}\right)=\frac{\partial}{\partial t}\left(Q_2\frac{gh^2}{2}\right)+\frac{\partial}{\partial x}\left(gh^2RU\right) \quad (90)$$

we can obtain the depth-averaged mechanical energy balance equation

$$\frac{\partial hRe_M}{\partial t}+\frac{\partial}{\partial x}\left(hRUe_M+\Pi U\right)=\mathcal{P}_{\rm int}+\mathcal{P}_{\rm ext} \quad (91)$$

where the mechanical energy is given by

$$e_M=\frac{U^2}{2}+\frac{W^2}{2}+\frac{\left(W-\dot{b}\right)^2}{6}+\frac{Q_2}{R}\frac{gh}{2}+gb \quad (92)$$

and the power related to internal forces is

$$\mathcal{P}_{\rm int}=P\left(2W+h\frac{\partial U}{\partial x}-2\dot{b}\right) \quad (93)$$

Internal force power is exchanged between the mechanical energy and internal energy of the system. The difference between the total energy conservation equation (82) and the mechanical energy balance equation (91) gives the depth-averaged internal energy balance equation

$$\frac{\partial hRe_{\rm int}}{\partial t}+\frac{\partial hRUe_{\rm int}}{\partial x}=-\mathcal{P}_{\rm int} \quad (94)$$

We notice that the right-hand side of this equation is a very small quantity because the expression (60) of $W$ implies that the sum of the three terms between brackets in the expression (93) of $\mathcal{P}_{\rm int}$ is equal to zero to within small terms. This means that equation (94) is a relaxation equation.

This equation is useful to find a suitable equation for the non-hydrostatic pressure $P$. The equation for $P$ was postulated by Escalante *et al.* (2019) [24] and by Escalante & Morales de Luna (2020) [25] for the incompressible case where $R=1$. In the present case of weakly compressible flow, the equation can also be regarded as postulated rather than derived unlike the three other equations. The postulate amounts to choosing the expression for the internal energy as

$$e_{\rm int}=\frac{P^2}{2a^2} \quad (95)$$

This expression is reminiscent of an acoustic energy. Inserting (95) into (94) and using the mass conservation equation (47) lead to $hRP\,\mathrm{D}P/\mathrm{D}t=-a^2P(2W+h\partial U/\partial t-2\dot{b})$, which gives the equation for $P$

$$\frac{\partial hRP}{\partial t}+\frac{\partial hRUP}{\partial x}=-a^2\left(2W+h\frac{\partial U}{\partial x}-2\dot{b}\right) \quad (96)$$

This equation has a special status in the model because it is a relaxation equation.

However, even if this equation is not really derived, it can be justified by the following considerations which show that it is consistent with the other equations of the model. In the exact mass conservation equation (52), since $\rho=\rho_H+\rho_N$ and $p_N=a^2\rho_N$, $\overline{\rho}$ can be written

$$\frac{\overline{\rho}}{\rho_s}=R+\frac{P}{a^2} \quad (97)$$

leading to

$$\frac{\partial}{\partial t}\left(h\frac{P}{a^2}\right)+\frac{\partial}{\partial x}\left(hU\frac{P}{a^2}\right)=-\left(\frac{\partial hR}{\partial t}+\frac{\partial hUR}{\partial x}\right) \quad (98)$$

This can be further simplified as follows, writing in dimensionless form with $R=1+O(\varepsilon^{2\gamma})$,

$$\varepsilon^{2+2\gamma}\left(\frac{\partial}{\partial t}\left(M_1^2hP\right)+\frac{\partial}{\partial x}\left(M_1^2hUP\right)\right)=-\left(\frac{\partial h}{\partial t}+U\frac{\partial h}{\partial x}+h\frac{\partial U}{\partial x}\right)+O(\varepsilon^{2\gamma})+O(\varepsilon^{\beta}) \quad (99)$$

The first two terms in the right-hand side of this equation can be written $-(2W-2\dot{b})$ using the kinematic boundary condition (5) and the asymptotic expression (59) of $w$. The $O(\varepsilon^{2\gamma})$ terms and the $O(\varepsilon^{\beta})$ terms are discarded because the corrective terms of $O(\varepsilon^{2\gamma})$ and of $O(\varepsilon^{\beta})$ are neglected in the expression of $W$ (60), and thus in the relaxation. The equation of $P$ is postulated rather than rigorously derived because the $O(\varepsilon^{2+2\gamma})$ terms are not neglected. The fact that the $O(\varepsilon^{2+2\gamma})$ terms appear on the left-hand side of equation (99) is solely to ensure the model is hyperbolic, and does not affect its compressible properties. Without these terms, the model is still an extension of the Serre-Green-Naghdi equations to compressible flows but it is not hyperbolic. The hyperbolicity results from a postulate as it is also the case for all hyperbolic approximations of the Serre-Green-Naghdi system (see Favrie & Gavrilyuk 2017 [22] or Escalante *et al.* 2019 [24] for example).

Using once more $R=1+O(\varepsilon^{2\gamma})$ and reverting to dimensional form, we obtain equation (96).

It follows that the system of equations of the model admits an exact equation of energy conservation.

*2.3.5. Final system of equations*

In dimensional form the final system of equations is

$$\frac{\partial h}{\partial t}+\frac{\partial hU}{\partial x}=\frac{M^2}{2}Q_0h\frac{\partial U}{\partial x} \quad (100)$$

$$\frac{\partial hR\mathcal{U}}{\partial t}+\frac{\partial}{\partial x}\left(hRU\mathcal{U}+Q_1\frac{gh^2}{2}+hP\right)=-\left(ghR+\frac{3}{2}P\right)\frac{\partial b}{\partial x}+hR\frac{\dot{b}}{4}\frac{\mathrm{D}}{\mathrm{D}t}\left(\frac{\partial b}{\partial x}\right) \quad (101)$$

$$\frac{\partial hR\mathcal{W}}{\partial t}+\frac{\partial hRU\mathcal{W}}{\partial x}=\frac{3}{2}P \tag{102}$$

$$\frac{\partial hRP}{\partial t}+\frac{\partial hRUP}{\partial x}=-a^2\left(2W+h\frac{\partial U}{\partial x}-2\dot{b}\right) \tag{103}$$

with $R$ given by (45), $M$ by (25), $Q_0$ by (50) and $Q_1$ by (55). This system admits the mass conservation equation

$$\frac{\partial hR}{\partial t}+\frac{\partial hUR}{\partial x}=0 \tag{104}$$

and the exact energy conservation equation (82). To the author's knowledge, this is the first model of this kind (i.e. Boussinesq-type models, here in a hyperbolic fully nonlinear version) where actual compressible effects are included. In this model, $\operatorname{div}\boldsymbol{v}\neq 0$ and the density is variable due to the hydrostatic corrections caused by depth variations. These compressible effects are noticeable in the case of tsunami propagation in deep water where the Mach number, as defined by (25), is in the 0.1–0.2 range.

For coastal waves, this Mach number is smaller than $10^{-2}$ and a quasi-incompressible approximation is sufficient. This approximation can be found by putting $M=0$ in the system (100)–(103), which implies $R=Q_0=Q_1=1$. Note that the sound velocity $a$ in the relaxation term at the right-hand side of equation (103) is retained to ensure the hyperbolicity of the resulting set of equations. Putting $a\to\infty$ in this equation would give the Serre-Green-Naghdi equations. The quasi-incompressible set of equations is thus written

$$\frac{\partial h}{\partial t}+\frac{\partial hU}{\partial x}=0 \tag{105}$$

$$\frac{\partial h\mathcal{U}}{\partial t}+\frac{\partial}{\partial x}\left(hU\mathcal{U}+\frac{gh^2}{2}+hP\right)=-\left(gh+\frac{3}{2}P\right)\frac{\partial b}{\partial x}+h\frac{\dot{b}}{4}\frac{\mathrm{D}}{\mathrm{D}t}\left(\frac{\partial b}{\partial x}\right) \tag{106}$$

$$\frac{\partial h\mathcal{W}}{\partial t}+\frac{\partial hU\mathcal{W}}{\partial x}=\frac{3}{2}P \tag{107}$$

$$\frac{\partial hP}{\partial t}+\frac{\partial hUP}{\partial x}=-a^2\left(2W+h\frac{\partial U}{\partial x}-2\dot{b}\right) \tag{108}$$

The quasi-incompressible character of this system is obvious when looking at the mass conservation equation (105) which is the classical depth-integrated form of $\operatorname{div}\boldsymbol{v}=0$. This quasi-incompressible model also satisfies an exact equation of energy conservation, which is (82), together with the expressions (81), (83) and (84), with $R=Q_1=Q_2=1$.

In the quasi-incompressible system, it is possible to choose an artificially smaller value of the sound velocity in order to decrease the computational time. This possibility is similar to the method, used by several authors (Auclair *et al.* 2018 for example), of adding an artificial compressibility to the system for better numerical efficiency. This method transforms the quasi-incompressible system into a hyperbolic approximation of the Serre-Green-Naghdi equations, which is not the case for the compressible model (100)–(103). The sound velocity $a$ can be considered in this system as a free parameter which should have a sufficiently large value in order to obtain an accurate approximation of the Serre-Green-Naghdi equations. In this regard, the quasi-incompressible model is similar to those of Favrie & Gavrilyuk (2017) [22], Escalante *et al.* (2019) [24], Escalante & Morales de Luna (2020) [25] and Bassi *et al.* (2020) [26].

However, the treatment of the variable bottom terms in the quasi-incompressible system is new because an arbitrary bathymetry is handled with only four equations and a change of variables instead of the six equations required by the approaches of Escalante & Morales de Luna (2019) [25] or Bassi *et al.* (2020) [26].

The applications of both types of model are different. The compressible model is intended for the simulation of tsunami propagation whereas the quasi-incompressible equations are well-suited to the simulation of coastal waves. In both cases, breaking effects could be readily included in the models using the approach of Kazakova & Richard (2019) [48] but this is left for future work.

The mild slope approximation is obtained by assuming that the characteristic variation length of the bottom is much larger that $L$, for example $L/\varepsilon$ or $L/\varepsilon^2$. In this case, all bathymetric terms, are negligible except $-p_H(b)\partial b/\partial x$ in (101). Assuming in addition that the bottom is fixed, the model for a mild bottom is composed of the mass equation (100) and

$$\frac{\partial hRU}{\partial t}+\frac{\partial}{\partial x}\left(hRU^2+Q_1\frac{gh^2}{2}+hP\right)=-ghR\frac{\partial b}{\partial x} \tag{109}$$

$$\frac{\partial hRW}{\partial t}+\frac{\partial hRUW}{\partial x}=\frac{3}{2}P \tag{110}$$

$$\frac{\partial hRP}{\partial t}+\frac{\partial hRUP}{\partial x}=-a^2\left(2W+h\frac{\partial U}{\partial x}\right) \tag{111}$$

As above the quasi-incompressible model for a fixed mild slope bottom is found by putting $M=0$ and $R=Q_0=Q_1=1$ in these equations. In all these models, an exact energy conservation equation is satisfied.

## 3. Model analysis

### *3.1. Hyperbolicity*

The system (100)–(103) can be written

$$\frac{\partial\overline{\mathbf{V}}}{\partial t}+\overline{\overline{\mathbf{A}}}\,\frac{\partial\overline{\mathbf{V}}}{\partial x}=\overline{\mathbf{S}} \tag{112}$$

where $\overline{\mathbf{V}}=(h,\mathcal{U},\mathcal{W},P)^{\mathrm{T}}$, $\overline{\mathbf{S}}$ is a source term depending on $b$ and its derivatives, and on $h$, $\mathcal{U}$, $\mathcal{W}$, $P$ but not on

their derivatives, and where

$$\overline{\overline{\mathbf{A}}} = \begin{bmatrix} U & \mathrm{e}^{-M^2} hRK_b & 0 & 0 \\ g + P/(hR) & U & 0 & 1/R \\ 0 & 0 & U & 0 \\ 0 & K_b a^2/R & 0 & U \end{bmatrix} \tag{113}$$

with

$$K_b = \frac{1}{1 + \dfrac{1}{4}\left(\dfrac{\partial b}{\partial x}\right)^2} \tag{114}$$

The eigenvalues of $\overline{\overline{\mathbf{A}}}$ are

$$\lambda_{1,2} = U$$
$$\lambda_{3,4} = U \pm \sqrt{K_b}\sqrt{\mathrm{e}^{-M^2}\left(ghR + P\right) + \frac{a^2}{R^2}} \tag{115}$$

Since $P/(gh) = O(\varepsilon^2)$ and since the physical value of the sound velocity $a = 1500\,\mathrm{m}\cdot\mathrm{s}^{-1}$ is such that $a^2$ is always much larger than $gh$ or $|P|$, the eigenvalues are real. In the case of the quasi-incompressible system with an artificially reduced value of the sound velocity, $a$ should be chosen large enough to ensure the existence of real eigenvalues. In practice this is not restrictive because $|P|$ is always small enough so that the eigenvalues are always real. Because of the double root, the system is not strictly hyperbolic but it is possible to find four linearly independent eigenvectors. The system is thus hyperbolic.

Wave celerity is smaller for free surface waves travelling over a variable bed than over a uniform bed because the celerity is multiplied by $\sqrt{K_b}$ and $K_b \leqslant 1$. In practice however, $(\partial b/\partial x)^2$ is often small and the surface wave velocity is only slightly decreased except for very steep bottom slopes. For example, if the bottom slope is 1/10, 1/5 and 1, $\sqrt{K_b}$ is equal to 0.999, 0.995 and 0.894 respectively.

For the quasi-incompressible model, the eigenvalues reduce to $\lambda_{1,2} = U$ and $\lambda_{3,4} = U \pm \sqrt{K_b}\sqrt{gh + P + a^2}$.

### *3.2. Dispersive properties*

The linear dispersive properties of the model are studied from the derivation of the dispersion relation for the system of equations (100)–(103) in the case of a constant bottom. These equations are linearized around the equilibrium state $h_0$, $R_0 = [\exp(M_0^2) - 1]/M_0^2$, $U_0 = 0$, $W_0 = 0$ and $P_0 = 0$ considering small perturbations $h'$, $U'$, $W'$ and $P'$. These perturbations are taken of the form

$$[h', U', W', P']^{\mathrm{T}} = [A_1, A_2, A_3, A_4]^{\mathrm{T}}\,\mathrm{e}^{\mathrm{i}(kx - \omega t)} \tag{116}$$

leading to the dispersion relation

$$\frac{h_0^2 R_0^2}{3a^2}\omega^4 - \omega^2\left[1 + \frac{k^2 h_0^2}{3}\left(1 + M_0^2 \mathrm{e}^{-M_0^2} R_0^3\right)\right] + \mathrm{e}^{-M_0^2} k^2 g h_0 R_0 = 0 \tag{117}$$

In dimensionless form, for low frequencies $\varepsilon\tilde{\omega} = \omega\sqrt{h_0/g}$ and with the longwave scaling $\varepsilon\tilde{k} = kh_0$, the dispersion relation is

$$\tilde{\omega}^2\left(1 + \varepsilon^2\frac{\tilde{k}^2}{3}\right) = \mathrm{e}^{-M_0^2} R_0 \tilde{k}^2 + O(\varepsilon^{2+2\gamma}) \tag{118}$$

If $\gamma = 1$, $M_0^2 = \varepsilon^2 M_1^2$, then, at the order $O(1)$, the dispersion relation reduces to $\tilde{\omega}^2 = \tilde{k}^2$ giving the phase velocity of the incompressible Saint-Venant equations $v_\varphi = \sqrt{gh_0}$. At the following order $O(\varepsilon^2)$, the dispersion relation can be developed into

$$\tilde{\omega}^2 = \tilde{k}^2\left(1 - \varepsilon^2\frac{M_1^2}{2} - \varepsilon^2\frac{\tilde{k}^2}{3}\right) + O(\varepsilon^4) \tag{119}$$

If $\gamma = 1/2$, $M_0^2 = \varepsilon M_1^2$, then the dispersion relation reduces at order $O(\varepsilon)$ to

$$\tilde{\omega}^2 = \tilde{k}^2 \mathrm{e}^{-M_0^2} R_0 \tag{120}$$

which can be written

$$\tilde{\omega}^2 = \tilde{k}^2\left(1 - \varepsilon\frac{M_1^2}{2}\right) + O(\varepsilon^2) \tag{121}$$

At the following order, the dispersion relation is

$$\tilde{\omega}^2 = \tilde{k}^2\left(1 - \varepsilon\frac{M_1^2}{2} + \varepsilon^2\frac{M_1^4}{6} - \varepsilon^2\frac{\tilde{k}^2}{3}\right) + O(\varepsilon^3) \tag{122}$$

All these expresions show that, even at the long wave limit, the dispersion relation is modified by compressibility effects. The phase velocity for $k \to 0$ is thus

$$v_\varphi = \sqrt{gh_0 \mathrm{e}^{-M_0^2} R_0} \tag{123}$$

which is practically

$$v_\varphi \simeq \sqrt{gh_0}\left(1 - \frac{M_0^2}{4}\right) \tag{124}$$

for $2\gamma = 2$, and

$$v_\varphi \simeq \sqrt{gh_0}\left(1 - \frac{M_0^2}{4} + \frac{5M_0^4}{96}\right) \tag{125}$$

for $2\gamma = 1$. Compared to the incompressible case, the phase velocity is slightly smaller due to the compressibility of water. For typical ocean depths, this diminution of the phase velocity is of the order of 0.5 %.

The dispersion relation in the linear theory of compressible fluids is (Pidduck 1910 [50], Dalrymple & Rogers 2007 [51], Kadri 2015 [52], Abdolali & Kirby 2017 [37])

$$\omega^2 = g\frac{\left(\kappa^2 - \Gamma^2\right)\tanh(\kappa h_0)}{\kappa - \Gamma\tanh(\kappa h_0)} \tag{126}$$

where $\Gamma = g/(2a^2)$ and $\kappa = \sqrt{k^2 - \omega^2/a^2 + \Gamma^2}$. Using the same low frequency and long wave scaling as above (the

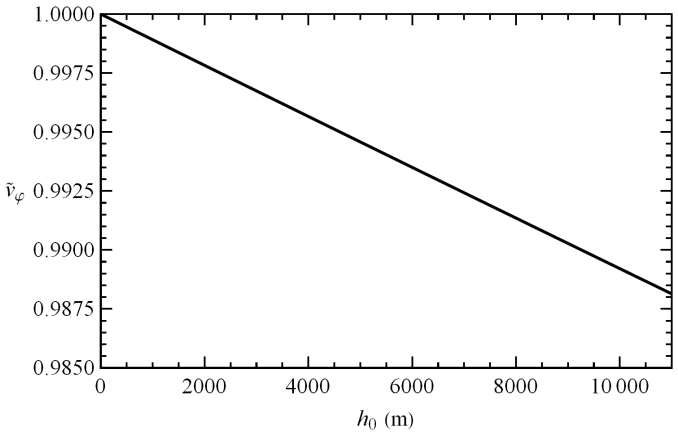


Figure 2: Dimensionless phase velocity $v_\varphi/\sqrt{gh_0}$ as a function of the depth $h_0$.

low frequency scaling eliminating the acoustic modes) and $M_0 = O(\varepsilon^{2\gamma})$, this dispersion relation gives exactly the same relation dispersion as the model: If $\gamma = 1$, (126) gives (119) and if $\gamma = 1/2$, (126) gives (122). At the limit $\gamma \to 0$, which is the longwave limit where the compressible effects are much larger than the dispersive effects, the dispersion relation (126) of the linear theory reduces to

$$\tilde{\omega}^2 = \frac{\left(\tilde{k}^2 - \varepsilon^{2\gamma} M_1^2 \tilde{\omega}^2\right) \tanh\left(\varepsilon^{2\gamma} M_1^2/2\right)}{\left(\varepsilon^{2\gamma} M_1^2/2\right)\left(1 - \tanh\left(\varepsilon^{2\gamma} M_1^2/2\right)\right)} + O(\varepsilon^2) \qquad (127)$$

The solution of this equation can be written

$$\tilde{\omega}^2 = \tilde{k}^2 \mathrm{e}^{-M_0^2} R_0 + O(\varepsilon^2) \qquad (128)$$

which is the same expression as given by the model for the same scaling and the same limit. It follows that the phase velocity at the long wave limit with compressible effects is the same in the model and in the linear theory and its expression is (123). This is also the expression of the group velocity because, at this limit, there is no dispersion. In the development of (123)

$$\frac{v_\varphi}{\sqrt{gh_0}} = 1 - \frac{M_0^2}{4} + \frac{5}{96} M_0^4 - \frac{M_0^6}{128} + O(M_0^8) \qquad (129)$$

only terms of order $n$ in $M_0^2$ with $n = 1/\gamma$ have meaning because the first dispersive term is $O(\varepsilon^2)$. This implies that, in practice, the expressions (124) or (125) are sufficient and consistent. The variation of the dimensionless phase velocity $v_\varphi/\sqrt{gh_0}$ with depth is shown in figure 2 ($a = 1500\,\mathrm{m}\cdot\mathrm{s}^{-1}$). This variation is almost linear with $h_0$ because it is well approximated by (124) which gives $\tilde{v}_\varphi \simeq 1 - gh_0/(4a^2)$. In most cases the relative diminution in phase velocity due to compressibility is smaller than 1 %.

The model is thus fully consistent with the general linear theory of compressible fluids with respect to compressible effects at the long wave limit. It is also consistent to the first order in $k^2$ for dispersive effects in the same way as the incompressible Serre-Green-Naghdi model.

The complete dispersion relation (117) can be explicitly solved. The solutions of this equation divide into a slow branch and a fast branch. Their expressions are given by

$$\tilde{\omega}^2 = \frac{1}{2M_0^2 R_0^2}\left[3 + \tilde{k}^2\left(1 + M_0^2 R_0^3 \mathrm{e}^{-M_0^2}\right) \pm \sqrt{\left(3 + \tilde{k}^2\right)^2 + \frac{2M_0^2 R_0^3}{\mathrm{e}^{M_0^2}}\tilde{k}^2\left(\tilde{k}^2 - 3\right) + \frac{M_0^4 R_0^6}{\mathrm{e}^{2M_0^2}}\tilde{k}^4}\right] \qquad (130)$$

with the minus sign for the slow branch and the plus sign for the fast branch. Since the fast branch corresponds to an acoustic mode and the slow branch to the usual solution in hydraulics of free surface flows but for the compressible corrections, they will be also called thereafter the acoustic branch and the hydraulic branch respectively. These solutions are presented in figure 3 for $h_0 = 6000\,\mathrm{m}$ with the angular frequency and the phase velocity of both branches as a function of $\tilde{k}$ in figure 3 (a) and (b) respectively. The acoustic branch has a cutoff frequency $\tilde{\omega}_c = \sqrt{3}/(M_0 R_0)$ or, in dimensional form,

$$\omega_c = \frac{a\sqrt{3}}{R_0 h_0} \qquad (131)$$

which is the angular frequency of the fast branch at $k = 0$. There is no acoustic mode at a lower frequency. The phase velocity of the acoustic mode, denoted by $v_\varphi^a$, can be written

$$\tilde{v}_\varphi^a = \frac{1}{M_0 R_0}\sqrt{1 + \frac{3}{\tilde{k}^2}} + O(M_0)$$
$$v_\varphi^a \simeq \frac{a}{R_0}\sqrt{1 + \frac{3}{k^2 h_0^2}} \qquad (132)$$

This velocity is infinite when $M_0 = 0$ (or $a \to \infty$), which is the incompressible limit, and decreases monotonously when the Mach number, or the wave number, increases. In practice, the value of the acoustic phase velocity is slightly higher than the value given by the above expression, due to the corrective term of $O(M_0)$. When $\tilde{k} \to 0$, $\tilde{v}_\varphi^a \to \infty$ but the group velocity of the acoustic mode vanishes (the group velocity of the acoustic mode is equal to 0 for $k = 0$). This is due to the existence of the cutoff frequency $\omega = \omega_c$ for $k = 0$. At this point, there is no energy propagation in the acoustic mode. The group velocity of the acoustic mode increases with $\tilde{k}$ and is smaller than the sound velocity (see the dashed curve in figure 3).

In the case of the quasi-incompressible model, the dispersive properties are the same as for the Serre-Green-Naghdi equations if the physical value of the sound velocity is used. However this leads to a very small time step and a large computational time due to the large value of the sound velocity in water. An artificially reduced sound

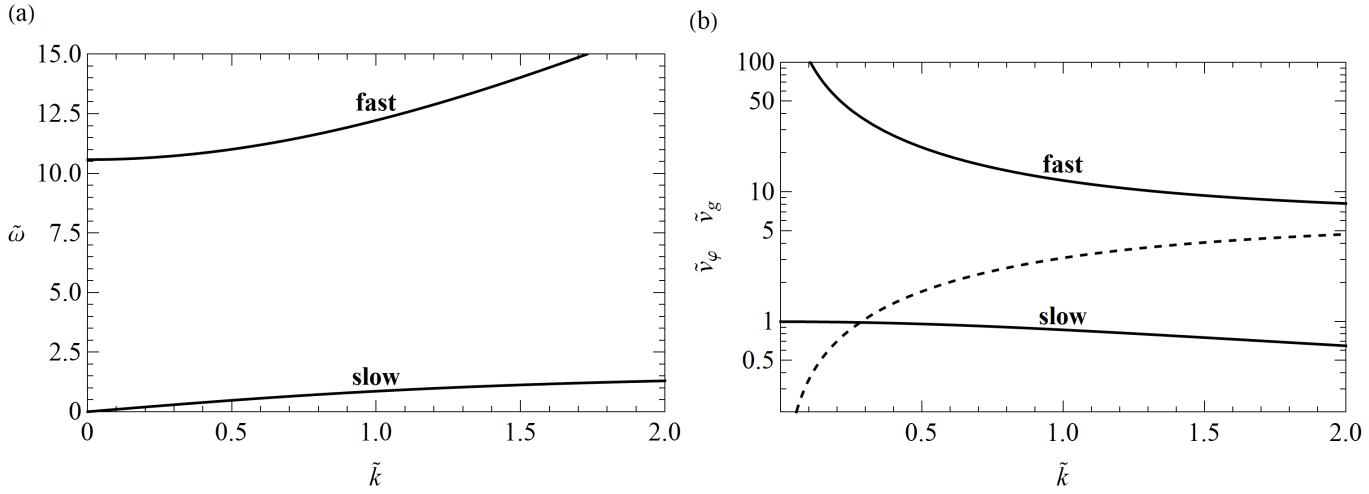


Figure 3: Solutions of the relation dispersion with the fast or acoustic branch and the slow or hydraulic branch for $h_0 = 6000\,\mathrm{m}$: (a) angular frequency and (b) phase velocity. The dashed curve in (b) is the group velocity of the acoustic branch.

velocity can be used giving the same dispersive properties with an excellent approximation as long as $M_0 \leqslant 0.1$, which gives a much reduced computational time with the same accuracy.

### *3.3. Soliton*

The system (100)–(103) admits soliton solutions in the case of a uniform, horizontal bed. A soliton propagates at a constant velocity $c$ and is thus a stationary solution in a reference frame in translation at this velocity with respect to the reference frame of the bottom. We are looking for a function of the variable $\xi = x - ct$ satisfying $h \to h_\infty$, $U \to 0$, $W \to 0$, $P \to 0$ and $R \to R_\infty$ if $\xi \to \pm\infty$ where $U$ is the average horizontal velocity in the reference frame of the bottom and $R_\infty$ is the value of $R$ for $h = h_\infty$.

Given that $\partial/\partial t = -c\mathrm{d}/\mathrm{d}\xi$ and $\partial/\partial x = \mathrm{d}/\mathrm{d}\xi$, the mass conservation equation (104) implies that the relative discharge

$$\overline{m} = hR\,(U - c) \tag{133}$$

is a constant. The momentum balance equation in the horizontal direction (101) with a constant bottom yields another constant $B$ defined by

$$B = \frac{\overline{m}^2}{hR} + Q_1\frac{gh^2}{2} + hP \tag{134}$$

The energy equation (82) gives a third constant $\overline{H}$, which writes

$$\overline{H} = \frac{\overline{m}^2}{2h^2R^2} + \frac{2}{3}W^2 + gh + \frac{P^2}{2a^2} + \frac{P}{R} \tag{135}$$

The expression of the non-hydrostatic pressure can be found from (134):

$$P = \frac{B}{h} - \frac{\overline{m}^2}{h^2R} - Q_1\frac{gh}{2} \tag{136}$$

The non-hydrostatic pressure equation (103) and the expression of $P$ above gives an expression for the average vertical velocity

$$W = \overline{m}\left(\frac{Q_4}{2h} + \frac{B}{2a^2h^2} - Q_5\frac{\overline{m}^2}{a^2h^3} + Q_1\frac{g}{4a^2}\right)\frac{\mathrm{d}h}{\mathrm{d}\xi} \tag{137}$$

where

$$Q_4 = \frac{M^4}{4\sinh^2(M^2/2)} = 1 + O(M^4) \tag{138}$$

and

$$Q_5 = \frac{M^2}{2}\frac{\left(1+M^2\right)\mathrm{e}^{M^2} - 1}{\left(\mathrm{e}^{M^2} - 1\right)^2} = 1 - \frac{M^2}{4} + O(M^4) \tag{139}$$

The equations are put into dimensionless form by defining $\hat{h} = h/h_\infty$, $\hat{\xi} = \xi/h_\infty$, $\hat{P} = P/gh_\infty$ and two dimensionless numbers, the Mach number $M_\infty = \sqrt{gh_\infty}/a$ and the relative Froude number $\overline{F}_\infty = -\overline{m}/\sqrt{gh_\infty^3}$. The constants $B$ and $\overline{H}$ can be evaluated for $\xi \to \pm\infty$. This gives

$$B = gh_\infty^2\left(\frac{\overline{F}_\infty^2}{R_\infty} + \frac{Q_{1\infty}}{2}\right), \quad \overline{H} = gh_\infty\left(\frac{\overline{F}_\infty^2}{2R_\infty^2} + 1\right) \tag{140}$$

where $Q_{1\infty}$ is the value of $Q_1$ for $h = h_\infty$. These expressions, used with the energy conservation (135) and the expressions (136) and (137) of $P$ and $W$, lead to the equation

$$f_1^2(\hat{h})\left(\frac{\mathrm{d}\hat{h}}{\mathrm{d}\hat{\xi}}\right)^2 - f_2(\hat{h}) = 0 \tag{141}$$

where

$$f_1(\hat{h}) = \frac{\overline{F}_\infty}{\sqrt{3}}\left[Q_4 + \frac{M_\infty^2}{\hat{h}}\left(\frac{\overline{F}_\infty^2}{R_\infty} + \frac{Q_{1\infty}}{2}\right) - 2\frac{M_\infty^2}{\hat{h}^2}Q_5\overline{F}_\infty^2 + Q_1\frac{M_\infty^2}{2}\hat{h}\right] \quad (142)$$

and

$$f_2(\hat{h}) = \frac{\overline{F}_\infty^2}{R^2} - \frac{Q_2}{R}\hat{h}^3 - \left(2\frac{\overline{F}_\infty^2}{R_\infty} + Q_{1\infty}\right)\frac{\hat{h}}{R} + \left(\frac{\overline{F}_\infty^2}{R_\infty^2} + 2\right)\hat{h}^2 - M_\infty^2\left(\frac{\overline{F}_\infty^2}{R_\infty} + \frac{Q_{1\infty}}{2} - \frac{\overline{F}_\infty^2}{\hat{h}R} - Q_1\frac{\hat{h}^2}{2}\right)^2 \quad (143)$$

For the maximum depth $h_{\max}$ of the solitary wave, $f_2(\hat{h}) = 0$. Apart from the root $\hat{h} = 1$, the positive root of this equation gives the maximum depth of the soliton. The dimensionless amplitude of the soliton is $h_{\max} - 1$. If $M_\infty = 0$, the maximum depth of the soliton of the Serre-Green-Naghdi equations is recovered. If $M_\infty$ increases, the amplitude of the soliton decreases. This implies that the soliton of the compressible model is slightly smaller than the soliton of the incompressible model (see figure 4(a) for a comparison between the incompressible and compressible cases for $M_\infty = 0.13$). The soliton of the incompressible equations exists if $\overline{F}_\infty > 1$. There is also a minimum value of the Froude number for the existence of the soliton of the compressible equations and this value is slightly greater than 1 (about $\overline{F}_\infty > 1.004$ if $M_\infty = 0.13$). The maximum depth of the soliton as a function of the Mach number $M_\infty$ is presented in figure 4(b) for a Froude number $\overline{F}_\infty \simeq 1.342$ ($\overline{F}_\infty^2 = 1.8$). The dashed curve is the quasi-incompressible case. As the quasi-incompressible case is a hyperbolic approximation of the incompressible Serre-Green-Naghdi equations, the value of the sound velocity should be chosen large enough to give approximately the same amplitude as the incompressible model (i.e. $M_\infty$ should be small enough). Note that in the quasi-incompressible case, $M_\infty$ appears only because of the presence of the sound velocity in the relaxation term in (108). The problem is completely different for the compressible equations (100)–(103), which are not an approximation of the incompressible equations, and where the slight decrease of the soliton amplitude is due to the inclusion of compressibility in the model.

Taking the derivative of the equation (141) leads to the equation

$$\frac{\mathrm{d}^2\hat{h}}{\mathrm{d}\hat{\xi}^2} + \frac{1}{f_1(\hat{h})}\frac{\mathrm{d}f_1}{\mathrm{d}\hat{h}}\left(\frac{\mathrm{d}\hat{h}}{\mathrm{d}\hat{\xi}}\right)^2 - \frac{1}{2f_1^2(\hat{h})}\frac{\mathrm{d}f_2}{\mathrm{d}\hat{h}} = 0 \quad (144)$$

which is more suitable for a numerical integration. The depth profile of a very steep soliton with $\overline{F}_\infty^2 = 1.8$ and $M_\infty = 0.13$ is presented in figure 5(a) (solid curve). This profile is very similar to the profile of the Serre-Green-Naghdi soliton (dashed curve) for the same Froude number. This soliton has a very large amplitude for an important Mach number, and thus a large still water depth, which is not realistic. For a more realistic soliton depicting a tsunami in a large depth (about 4000 m), the Mach number is $M_\infty \simeq 0.13$ but $\overline{F}_\infty^2$ is very close to 1. In the incompressible case, which can provide an order of magnitude, the dimensionless amplitude $h_{\max} - 1$ of the soliton is $\overline{F}_\infty^2 - 1$. For a tsunami in deep ocean, the amplitude is very small compared to the ocean depth which implies that $\overline{F}_\infty^2 - 1$ is small. The case of a soliton with more realistic values $\overline{F}_\infty^2 = 1.01$ and $M_\infty = 0.13$, is presented in figure 5 (b) (solid curve) with a comparison to the Serre-Green-Naghdi soliton at the same Froude number (dashed curve). The decrease in amplitude due to compressibility is notable.

## 4. Model with improved dispersive properties

### *4.1. Derivation*

The Boussinesq-type models are weakly dispersive (see for example Kirby 2016 [8]) and their dispersive properties can be inaccurate for some applications in coastal waves. Consequently various approaches improving the dispersive properties were proposed to extend the validity range of these models. Most operational Boussinesq-type models include some method to improve the dispersive properties (see for example Nwogu 1993 [10], Wei *et al.* 1995 [11], Kennedy *et al.* 2001 [12], Bonneton *et al.* 2011 [13]). The quasi-incompressible model has the same dispersive properties as the Serre-Green-Naghdi model if the Mach number is small enough and it is important to derive a version of the model with improved dispersive properties for accurate applications in coastal waves.

Besides coastal waves, the accuracy of the dispersive properties of the compressible model is also an important issue. Most earthquake-generated tsunamis have long wavelengths and thus small dispersive effects. However at long distances, dispersive effects are not negligible (Kirby *et al.* 2013 [40]). Furthermore tsunamis generated by submarine landslides have shorter wavelengths and consequently important dispersive effects even in the near field (Tappin *et al.* 2014 [53]). A study of the importance of dispersive effects for tsunami propagation can be found in Glimsdal *et al.* (2013) [41]. The model derived so far has accurate dispersive properties for long waves but these properties deteriorate quickly for shorter wavelengths and this deterioration is increased if the depth is larger due to more important compressible effects. As one of the purposes of this model is to capture a diminution of the phase velocity of only 0.5 % due to compressibility, the phase velocity and dispersive properties must be calculated to very high accuracy, even for tsunamis with a relatively short wavelength.

In this paper, the method of Bonneton *et al.* (2011) [13] is adapted for the present quasi-incompressible model for coastal wave applications. For the compressible model and

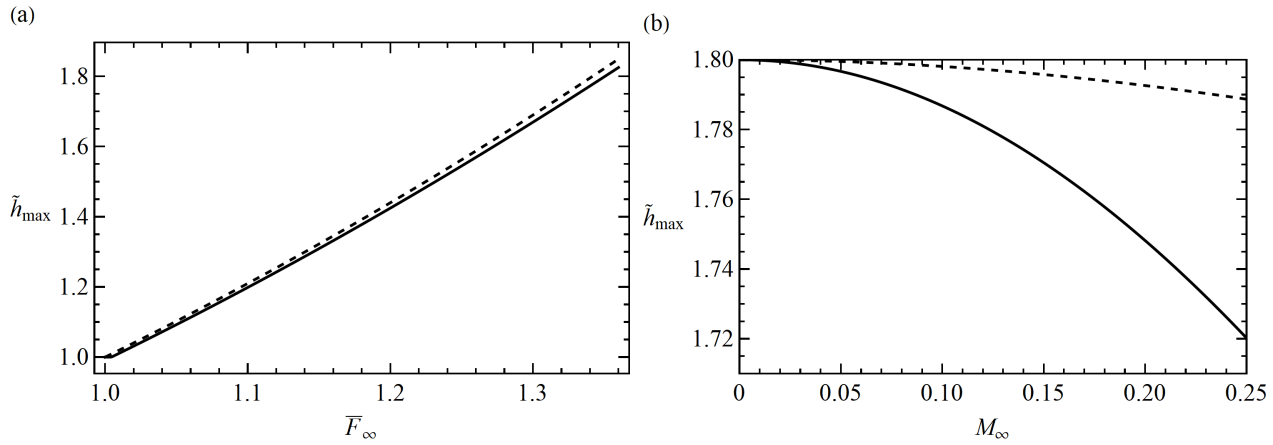


Figure 4: Dimensionless maximum depth of the soliton (a) as a function of $\overline{F}_\infty$ for $M_\infty = 0.13$ (solid curve) and (b) as a function of $M_\infty$ for $\overline{F}_\infty^2 = 1.8$ (solid curve). The dashed curve is in (a) the maximum depth of the soliton of the Serre-Green-Naghdi equations and in (b) the maximum depth in the quasi-incompressible case.

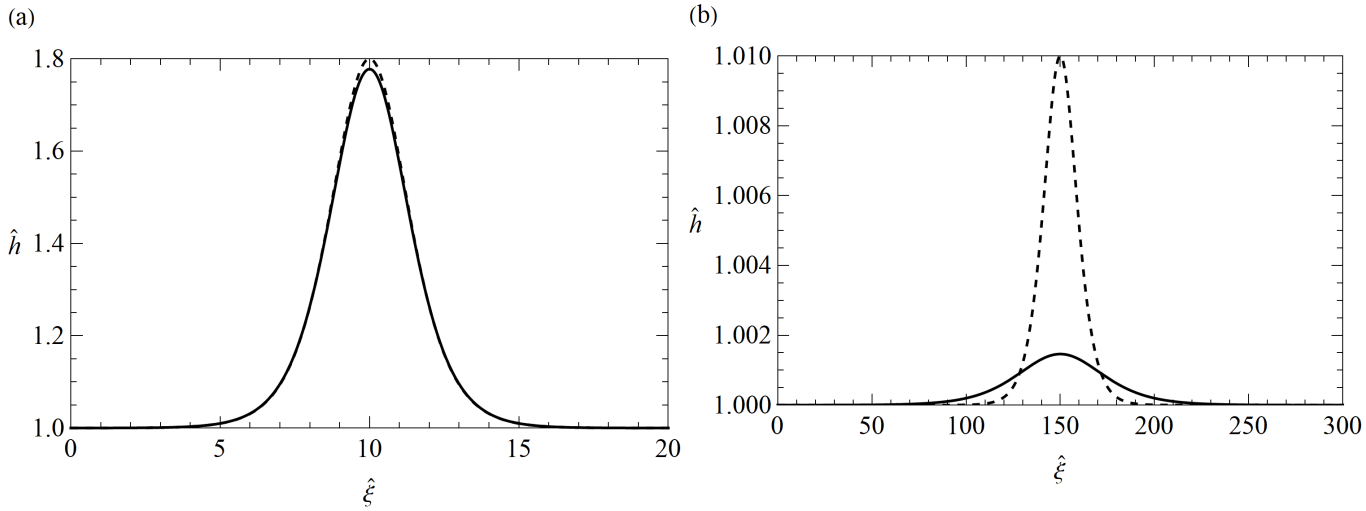


Figure 5: Profile of a soliton for the compressible equations with $M_\infty = 0.13$ (solid curve) and for the Serre-Green-Naghdi equations (dashed curve). (a) $\overline{F}_\infty^2 = 1.8$. (b) $\overline{F}_\infty^2 = 1.01$.

the specific case of tsunamis, Bonneton *et al.*'s method is not sufficient because improvement of the dispersive properties with this method alone depends heavily on the Mach number and thus is not satisfactory for all ocean depths. Consequently an additional correction is applied for the compressible effects.

Both corrections need to be consistent with respect to the asymptotic method used to derive the model. This means that the model with improve dispersive properties has to be asymptotically equivalent to the original model, differing only by terms of $O(\varepsilon^{2+2\gamma})$ or smaller.

The first idea is to use the vertical velocity at some height above the bottom as a variable instead of the average vertical velocity. More precisely the new variable $W^*$ is defined as the value of $w$ at a relative height $\alpha/2$ above the bottom with respect to the water depth i.e.

$$\frac{\alpha}{2} = \frac{z-b}{h} \tag{145}$$

This coefficient $\alpha$ coincides with the coefficient of the method of Bonneton *et al.* (2011) [13] but it has here a clear physical meaning. The definition

$$W^* = w|_{z=b+\alpha h/2} \tag{146}$$

and the asymptotic expression of $w$ (59) yields the asymptotic expression

$$\tilde{W}^* = -\frac{\alpha}{2}\tilde{h}\frac{\partial \tilde{U}}{\partial \tilde{x}} + \dot{b} + O(\varepsilon^{\beta}) + O(\varepsilon^{2\gamma}) \tag{147}$$

which leads to

$$\tilde{W}^* = \tilde{W} + \frac{1-\alpha}{2}\tilde{h}\frac{\partial \tilde{U}}{\partial \tilde{x}} + O(\varepsilon^{\beta}) + O(\varepsilon^{2\gamma}) \tag{148}$$

Consequently, defining

$$\mathcal{W}^* = W^* - \frac{\dot{b}}{4} \tag{149}$$

an equation for $\mathcal{W}^*$ can be obtained from the equation of $\mathcal{W}$. The resulting equation can be written

$$\frac{\partial hR\mathcal{W}^*}{\partial t} + \frac{\partial hRU\mathcal{W}^*}{\partial x} = \frac{3}{2}P + \frac{\alpha-1}{2}h^2R\left[2\left(\frac{\partial U}{\partial x}\right)^2 - \frac{\partial}{\partial x}\left(\frac{\mathrm{D}U}{\mathrm{D}t}\right)\right] \tag{150}$$

The key point of the approach of Bonneton *et al.* (2011) [13] is to use an asymptotically equivalent set of equations by noting that

$$\tilde{h}R\frac{\mathrm{D}\tilde{U}}{\mathrm{D}\tilde{t}} = -\frac{\partial}{\partial \tilde{x}}\left(\frac{Q_1\tilde{h}^2}{2}\right) - \tilde{h}R\frac{\partial \tilde{b}}{\partial \tilde{x}} + O(\varepsilon^2) + O(\varepsilon^{2\beta}) \tag{151}$$

which leads to $\mathrm{D}\tilde{U}/\mathrm{D}\tilde{t} = -\partial\tilde{Z}/\partial\tilde{x} + O(\varepsilon^2) + O(\varepsilon^{2\beta})$. Since the evolution equation of $W$ is accurate to within terms of $O(\varepsilon^{2\gamma})$ or $O(\varepsilon^{\beta})$, we can write to the same approximation, reverting to dimensional quantities,

$$\frac{\partial hR\mathcal{W}^*}{\partial t} + \frac{\partial hRU\mathcal{W}^*}{\partial x} = \frac{3}{2}P + \frac{\alpha-1}{2}h^2R\left[2\left(\frac{\partial U}{\partial x}\right)^2 + g\frac{\partial^2 Z}{\partial x^2}\right] \tag{152}$$

Replacing $W$ with its expression depending on $W^*$ in (103) gives the evolution equation of the average non-hydrostatic pressure

$$\frac{\partial hRP}{\partial t} + \frac{\partial hRUP}{\partial x} = -a^2\left(2W^* + \alpha h\frac{\partial U}{\partial x} - 2\dot{b}\right) \tag{153}$$

Equation (152) is difficult to solve because of the presence of the second derivative $\partial^2 h/\partial x^2$. To preserve a well-posed hyperbolic structure for the model, a new variable $S$, directly related to the slope of the free surface, is defined as

$$S = \alpha\frac{\partial Z}{\partial x} \tag{154}$$

An evolution equation for $S$ can be derived from the averaged mass conservation equation (100) which enables to write

$$\frac{\mathrm{D}}{\mathrm{D}t}\left(\frac{\partial h}{\partial x}\right) = -\frac{\partial}{\partial x}\left(\mathrm{e}^{-M^2}hR\frac{\partial U}{\partial x}\right) - \frac{\partial h}{\partial x}\frac{\partial U}{\partial x} \tag{155}$$

Using the asymptotic expression of $W^*$ (147) and the definition (154) of $S$, and neglecting terms of $O(\varepsilon^{2\gamma})$ in the equation of $S$ given that they would produce terms of $O(\varepsilon^{2+2\gamma})$ in the model, we obtain the evolution equation of $S$

$$\frac{\partial hRS}{\partial t} + \frac{\partial hRUS}{\partial x} = 2h\frac{\partial W^*}{\partial x} + \frac{2}{\alpha}W^*S + 2\frac{2-\alpha}{\alpha}\frac{\partial b}{\partial x}W^* + (\alpha-2)\,h\frac{\mathrm{D}}{\mathrm{D}t}\left(\frac{\partial b}{\partial x}\right) - \frac{2}{\alpha}\dot{b}\left[S + (2-\alpha)\frac{\partial b}{\partial x}\right] \tag{156}$$

The evolution equation of $\mathcal{W}^*$ (152) can thus be written, neglecting again terms of $O(\varepsilon^{2\gamma})$,

$$\frac{\partial hR\mathcal{W}^*}{\partial t} + \frac{\partial hRU\mathcal{W}^*}{\partial x} = \frac{3}{2}P + \frac{\alpha-1}{2\alpha}gh^2R\frac{\partial S}{\partial x} + 4\frac{\alpha-1}{\alpha^2}\left(W^* - \dot{b}\right)^2 \tag{157}$$

The quasi-incompressible model with improved dispersive properties is composed of the equations (105), (106) and of the equations (157), (153) and (156) with $R = 1$ and $Q_1 = 1$.

In the compressible case, the dispersive properties are indeed improved but either they are still not accurate enough for tsunamis or the value of the coefficient $\alpha$ giving accurate properties depends on the Mach number and thus on the depth. A new compressible correction is thus needed to supplement the above method.

Since $R = 1 + O(\varepsilon^{2\gamma})$, a term in equations (157), (153) or (156), which are accurate to within terms of $O(\varepsilon^{2\gamma})$, can be multiplied by $R$ without changing the accuracy of the model. We can rewrite consistently equations (157), (153) and (156) as

$$\frac{\partial hR\mathcal{W}^*}{\partial t} + \frac{\partial hRU\mathcal{W}^*}{\partial x} = \frac{3}{2}R^2 P + \frac{\alpha-1}{2\alpha} g h^2 R \frac{\partial S}{\partial x} + 4\frac{\alpha-1}{\alpha^2}\left(W^* - \dot{b}\right)^2 \quad (158)$$

$$\frac{\partial hRP}{\partial t} + \frac{\partial hRUP}{\partial x} = -a^2\left(2R^2 W^* + \alpha h \frac{\partial U}{\partial x} - 2\dot{b}\right) \quad (159)$$

$$\frac{\partial hRS}{\partial t} + \frac{\partial hRUS}{\partial x} = \frac{2h}{R^3}\frac{\partial W^*}{\partial x} + \frac{2}{\alpha}W^* S + 2\frac{2-\alpha}{\alpha}\frac{\partial b}{\partial x}W^* + (\alpha - 2)\, h \frac{\mathrm{D}}{\mathrm{D}t}\left(\frac{\partial b}{\partial x}\right) - \frac{2}{\alpha}\dot{b}\left[S + (2-\alpha)\frac{\partial b}{\partial x}\right] \quad (160)$$

The final compressible model with improved dispersive properties is composed of equations (100), (101), (158), (159) and (160). This model satisfies exactly the mass conservation equation (104). If $\alpha = 1$, the fifth equation (160) is useless and the system satisfies also exactly the energy conservation equation (82) with the same energy (83) and the same expression (81) of $\Pi$. The compressible correction, formed by the factor $R^2$ in the first term at the right-hand side of (158) and (159), preserves the exact conservation of energy. On the other hand, if $\alpha \neq 1$, the system has five equations and the energy conservation is not satisfied exactly but only asymptotically. This is the drawback of this method since there is the same problem in the incompressible case (see Bonneton *et al.* 2011 [13]).

In the case of a fixed bottom with a mild slope (see 2.3.5), all terms including $\partial b/\partial x$ or $\partial b/\partial t$ are removed except the term $-ghR\partial b/\partial x$ in (101). This also implies that $\mathcal{U} = U$ and $\mathcal{W}^* = W^*$.

### *4.2. Analysis*

#### *4.2.1. Hyperbolicity*

The system can be written

$$\frac{\partial \overline{\mathbf{V}}^*}{\partial t} + \overline{\overline{\mathbf{A}}}^* \frac{\partial \overline{\mathbf{V}}^*}{\partial x} = \overline{\mathbf{S}}^* \quad (161)$$

where $\overline{\mathbf{V}}^* = (h, \mathcal{U}^*, \mathcal{W}^*, P, S)^{\mathrm{T}}$, $\overline{\mathbf{S}}^*$ contains no derivatives of $h$, $\mathcal{U}^*$, $\mathcal{W}^*$, $P$ or $S$ and where the matrix $\overline{\overline{\mathbf{A}}}^*$ is given by (denoting $b_x = \partial b/\partial x$)

$$\begin{bmatrix} U & K_b \mathrm{e}^{-M^2} hR & 0 & 0 & 0 \\ g + \frac{P}{hR} & U & 0 & \frac{1}{R} & 0 \\ 0 & 0 & U & 0 & \frac{(1-\alpha)gh}{2\alpha} \\ 0 & \frac{K_b \alpha a^2}{R} & 0 & U & 0 \\ 0 & -\frac{K_b b_x}{2R^4} & -\frac{2}{R^4} & 0 & U \end{bmatrix} \quad (162)$$

The five eigenvalues of this matrix are

$$\lambda_1 = U \ ; \ \lambda_{2,3} = U \pm \frac{\sqrt{gh}}{R^2}\sqrt{\frac{\alpha-1}{\alpha}} \quad (163)$$

$$\lambda_{4,5} = U \pm \sqrt{K_b}\sqrt{(ghR + P)\,\mathrm{e}^{-M^2} + \frac{\alpha a^2}{R^2}} \quad (164)$$

The system is hyperbolic if $\alpha > 1$. Note that the value chosen by Bonneton *et al.* (2011) [13] is $\alpha = 1.159$ and satisfies this condition.

#### *4.2.2. Dispersive properties of the quasi-incompressible model*

The dispersive properties are studied with the same method as in §3.2 with a constant bottom and $S = 0$ in the equilibrium state used for the linearisation. Using the scaling $\tilde{\omega} = \omega\sqrt{h_0/g}$ and $\tilde{k} = kh_0$, the dispersion relation of the quasi-incompressible model is

$$\frac{M_0^2}{3}\tilde{\omega}^4 - \tilde{\omega}^2\left[1 + \frac{\tilde{k}^2}{3}\left(\alpha + \frac{2\alpha-1}{\alpha}M_0^2\right)\right] + \tilde{k}^2\left[1 + \tilde{k}^2\frac{\alpha-1}{3}\left(1 + \frac{M_0^2}{\alpha}\right)\right] = 0 \quad (165)$$

The value $\alpha = 1.159$ used by Bonneton *et al.* (2011) [13] in the incompressible model is appropriate for coastal waves. It gives accurate values of the phase velocity until $kh_0 \simeq 4$ and of the group velocity until $kh_0 \simeq 2.5$. The same results are obtained with the hyperbolic quasi-incompressible model. The relative deviation of the phase velocity with respect to the linear wave theory of Airy is presented in figure 6(a) (solid curves) as well as the relative deviation of the group velocity (dashed curves). The case of the Serre-Green-Naghdi equations is reproduced accurately with $\alpha = 1$ and $M_0 = 0.001$ (black curves). With $\alpha = 1.159$ and $M = 0.001$ (blue curves), the accuracy range of the phase velocity and of the group velocity is markedly increased as for the incompressible model of Bonneton *et al.* (2011) [13]. The phase and group velocities are almost the same with $M_0 = 0.1$ (orange curves), which implies that the computational time can be considerably shortened by decreasing artificially the sound velocity as long as $M_0 \leqslant 0.1$.

If the quasi-incompressible model with standard dispersive properties is used ($\alpha = 1$), the Mach number cannot be increased beyond 0.1 without deteriorating the dispersive properties. For instance, the case $\alpha = 1$ and $M_0 = 0.3$ is presented in figure 6(a) (grey curves), showing that the validity range of the model is decreased.

However, with the quasi-incompressible model with improved dispersive properties, the accuracy of the dispersive properties can be preserved with a value of the Mach number higher than 0.1 within certain limits. This remarkable property enables use of an even smaller sound velocity, which decreases even more the computational time. The cases $\alpha = 1.159$ and $M_0 = 0.2$ (green curves) and $\alpha = 1.159$ and $M_0 = 0.3$ (red curves) are presented in figure 6(a). A larger Mach number increases a little bit (in

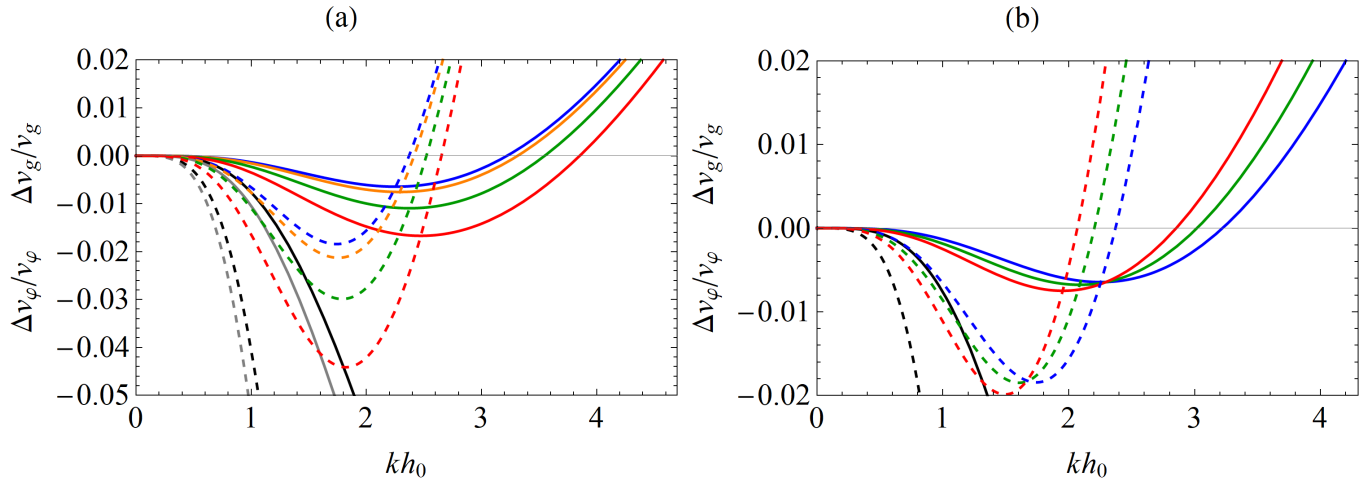


Figure 6: Relative deviation of the phase velocity (solid curves) and of the group velocity (dashed curves) for the quasi-incompressible model with respect to the linear wave theory of Airy. Black curves: $\alpha = 1$ and $M_0 = 0.001$; Blue curves: $\alpha = 1.159$ and $M_0 = 0.001$; Orange curves: $\alpha = 1.159$ and $M_0 = 0.1$; Grey curves: $\alpha = 1$ and $M_0 = 0.3$. (a): $\alpha = 1.159$ and $M_0 = 0.2$ (green); $\alpha = 1.159$ and $M_0 = 0.3$ (red). (b): $\alpha = 1.17$ and $M_0 = 0.2$ (green); $\alpha = 1.183$ and $M_0 = 0.3$ (red).

terms of absolute value) the deviation of the phase velocity for small values of $kh_0$ but decreases this deviation for larger values. If for example a tolerance of $\pm 2\%$ is taken, the validity range is actually increased with an increased value of $M_0$, as long as the Mach number does not exceed some maximum value. For the group velocity, the effect is the same although the increase of the deviation for small values of $kh_0$ is much more pronounced, which complicates the problem. The maximum value of $kh_0$ giving accurate values can be increased both for the phase velocity and for the group velocity at the cost of a larger deviation of the group velocity around $kh_0 \simeq 2$ (figure 6(a)). Another possibility is to keep the same accuracy of $\pm 2\%$ at the cost of a slightly reduced validity range. This case is presented in figure 6(b) with $\alpha = 1.17$ and $M_0 = 0.2$ (green curves), giving an accurate phase velocity until $kh_0 \simeq 3.9$ and an accurate group velocity until $kh_0 \simeq 2.45$, and with $\alpha = 1.183$ and $M_0 = 0.3$ (red curves) with an accurate phase velocity until $kh_0 \simeq 3.7$ and an accurate group velocity until $kh_0 \simeq 2.3$. In both cases, the computational time is significantly reduced.

*4.2.3. Dispersive properties of the compressible model*

In the case of the compressible model, using the same scaling as above, the dispersion relation is

$$\frac{M_0^2}{3R_0^2}\tilde{\omega}^4 - \tilde{\omega}^2\left(1 + \alpha\frac{\tilde{k}^2}{3R_0^4} + \frac{M_0^2}{3}\frac{\mathrm{e}^{-M_0^2}}{R_0}\tilde{k}^2 + \frac{\alpha-1}{\alpha}\frac{M_0^2}{3R_0^6}\tilde{k}^2\right) + \tilde{k}^2\left(R_0\mathrm{e}^{-M_0^2} + \frac{\alpha-1}{\alpha}\frac{M_0^2}{3}\frac{\mathrm{e}^{-M_0^2}}{R_0^5}\tilde{k}^2 + \frac{\alpha-1}{3}\frac{\tilde{k}^2}{R_0^8}\right) = 0 \tag{166}$$

For tsunamis the accuracy with the value $\alpha = 1.159$ used for coastal waves is not sufficient in the crucial range $0 \leqslant kh_0 \leqslant 1.5$. On the other hand, it is not necessary to keep a high accuracy until $kh_0 = 4$. Given that the compressibility entails a decrease of the phase velocity of about 0.5 %, a much higher accuracy is needed for the tsunamis wavelengths. The value which will be used thereafter is

$$\alpha = 1.19 \tag{167}$$

This value is larger than 1 and the system is thus hyperbolic. Note that this value is very close to the value $\alpha = 6/5$ which gives the (2,2) Padé approximant of the dispersion relation of the linear wave theory of Airy

$$\tilde{\omega}^2 = \tilde{k}^2\frac{1 + \tilde{k}^2/15}{1 + 2\tilde{k}^2/5} \tag{168}$$

The relative deviation of the phase velocity, defined by $(v_\varphi - v_\varphi^{\mathrm{lin}})/v_\varphi^{\mathrm{lin}}$ where $v_\varphi^{\mathrm{lin}}$ is the phase velocity given by the linear theory of compressible fluids (with the dispersion relation (126)), is presented in figure 7 for $h_0 = 2000\,\mathrm{m}$ (figure 7 (a)) and for $h_0 = 6000\,\mathrm{m}$ (figure 7 (b)). The black curve is the standard model (100)–(103), the blue curve is the energy-conserving model with improved dispersive properties and $\alpha = 1$ (i.e. the four equations (100), (101), (158) and (159) with $\alpha = 1$) and the red curve is the five-equation model (100), (101), (158), (159) and (160) with improved dispersive properties and $\alpha = 1.19$.

The standard model gives an accurate value for small wavelengths but the deviation at $kh_0 = 0.5$ is about 0.2 %, which is already too large to study tsunami propagation. The extended model with improved dispersive properties gives a very accurate value of the phase velocity until at least $kh_0 = 0.5$ if $\alpha = 1$ and $kh_0 = 1.5$ if $\alpha = 1.19$. For $h_0 = 6000\,\mathrm{m}$, the relative error is smaller than 0.1 % if $kh_0 \leqslant 0.37$ for the standard model, if $kh_0 \leqslant 0.68$ for the four-equation modified model with $\alpha = 1$ and if $kh_0 \leqslant 1.96$

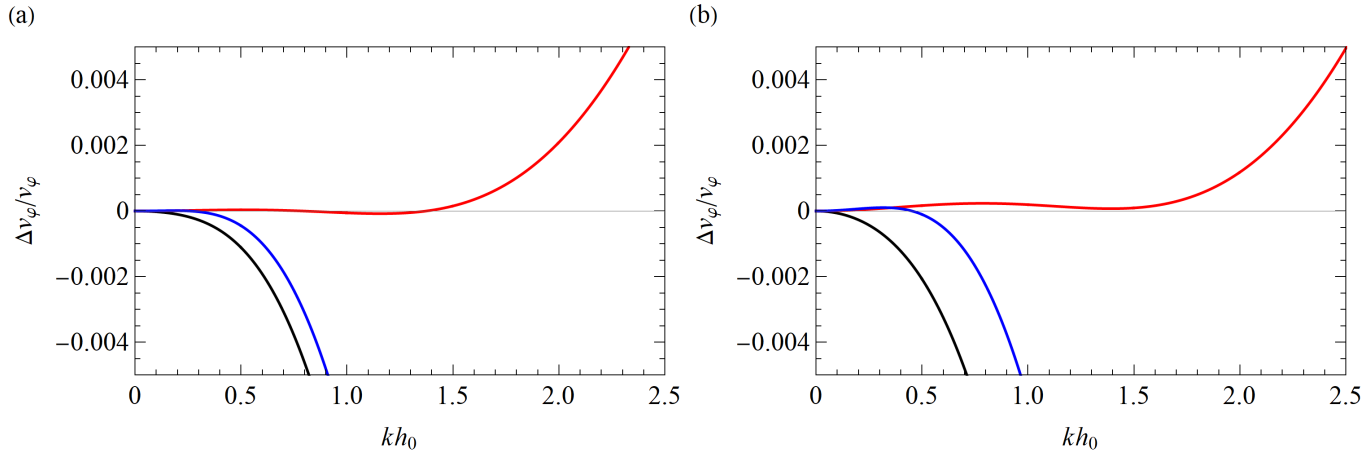


Figure 7: Relative deviation of the phase velocity with respect to the linear theory of compressible fluids for (a) $h_0 = 2000\,\mathrm{m}$ and (b) $h_0 = 6000\,\mathrm{m}$ : Model with standard dispersive properties (black), model with improved dispersive properties and $\alpha = 1$ (blue) and model with improved dispersive properties and $\alpha = 1.19$ (red).

for the five-equation extended model with $\alpha = 1.19$. The relative error given by the extended model with $\alpha = 1.19$ on the phase velocity is smaller than 0.03 % if $kh_0 \leqslant 1.5$. The relative deviation on the group velocity is also very small if $kh_0 \leqslant 1.5$ (smaller than 0.1 % in this range for $h_0 = 6000\,\mathrm{m}$). The phase velocity and the group velocity of the extended model are highly accurate for typical wavelengths of tsunamis for all depths which enables to capture the compressible effects on the propagation of tsunamis.

## 5. Numerical simulations

### *5.1. Pre-balanced formulation of the equations*

For the numerical resolution on an arbitrary bathymetry, the system must be well-balanced. The pre-balanced formulation of Rogers *et al.* (2001) [54], Rogers *et al.* (2003) [55], Liang & Marche (2009) [56] and Duran & Marche (2017) [57] is adapted to the case of compressible fluids. Using the variable $\eta = h - h_0$, the equations (100) and (101) write

$$\frac{\partial \eta}{\partial t} + \frac{\partial hU}{\partial x} = \frac{M^2}{2} Q_0 h \frac{\partial U}{\partial x} - \frac{\partial h_0}{\partial t} \tag{169}$$

$$\frac{\partial hR\mathcal{U}^*}{\partial t} + \frac{\partial}{\partial x}\left[hRU\mathcal{U}^* + Q_1 g\left(\frac{\eta^2}{2} + h_0\eta\right) + Q_1'\frac{gh_0^2}{2} + hP\right] = \left[g\left(h_0 R' + \eta R\right) + \frac{3}{2}P\right]\frac{\partial h_0}{\partial x} + hR\frac{\dot{h}_0}{4}\frac{\mathrm{D}}{\mathrm{D}t}\left(\frac{\partial h_0}{\partial x}\right) \tag{170}$$

where the following quantities are defined:

$$M_0^2 = \frac{gh_0}{a^2}\,; \quad R_0 = \frac{\mathrm{e}^{M_0^2} - 1}{M_0^2}$$
$$Q_{10} = \frac{2}{M_0^4}\left(\mathrm{e}^{M_0^2} - M_0^2 - 1\right)$$
$$Q_1' = Q_1 - Q_{10}\,; \quad R' = R - R_0 \tag{171}$$

The three other equations of the system are unchanged, keeping in mind that, in this case, $b = -h_0$. In the quasi-incompressible case, $M = M_0 = 0$, $R = R_0 = Q_1 = Q_{10} = 1$ and $R' = Q_1' = 0$. The numerical case of the lake at rest was used to test this pre-balanced formulation.

### *5.2. Numerical scheme*

The equations of the system are divided into a slow subsystem treated explicitly and a fast subsystem treated implicitly. This splitting is presented in table 1. Note that this implies that, in the fast subsystem, $\partial h/\partial t = 0$ and $\partial R/\partial t = 0$. This splitting is analogous to the splitting used by Tkachenko (2020) [58] and to the Horizontally Explicit Vertically Implicit (HEVI) UfPreb (U forward, Pressure backward) splitting of Weller *et al.* (2013) [59]. This forward-backward approach is based on Mesinger (1977) [60] and is a long-established practice for atmospheric models. In our case, the huge advantage of this approach is that no resolution of a global system is needed in the implicit step, which becomes computationally very cheap. In fact, with this splitting, the implicit step is cheaper than the explicit step in computational time.

A second-order scheme was implemented. The second order in space was obtained with a monotone upstream-centred scheme for conservation laws (MUSCL). Since there is no shock, no limiter is needed and none was used. Following Tkachenko (2020) [58] on a similar system, the second order in time was achieved with the diagonally-implicit Runge-Kutta (DIRK) Implicit-Explicit (IMEX) ARS2(2,2,2) scheme of Ascher *et al.* (1997) [61] (using the notation of Pareschi & Russo 2005 [62]). The ARS2(2,2,2) has two explicit stages and two implicit stages.

The implicit procedure used for the fast subsystem is a backward Euler method. The derivative $\partial U/\partial x$ is calculated by a central finite difference method.

In the explicit stages, the slow terms are computed by a finite volume method (Godunov-type) and a Rusanov Rie-

| *Slow subsystem* | *Fast subsystem* |
|---|---|
| $\dfrac{\partial \eta}{\partial t} + \dfrac{\partial hU}{\partial x} = \dfrac{M^2}{2} Q_0 h \dfrac{\partial U}{\partial x}$ | $\dfrac{\partial \eta}{\partial t} = -\dfrac{\partial h_0}{\partial t}$ |
| Equation (170) | $\dfrac{\partial U}{\partial t} = 0$ |
| $\dfrac{\partial hR\mathcal{W}^*}{\partial t} + \dfrac{\partial hRU\mathcal{W}^*}{\partial x} = \dfrac{\alpha - 1}{2\alpha} g h^2 R \dfrac{\partial S}{\partial x} + 4 \dfrac{\alpha - 1}{\alpha^2} \left( W^* + \dot{h}_0 \right)^2$ | $\dfrac{\partial hRW^*}{\partial t} = \dfrac{3}{2} R^2 P$ |
| $\dfrac{\partial hRP}{\partial t} + \dfrac{\partial hRUP}{\partial x} = 0$ | $\dfrac{\partial hRP}{\partial t} = -a^2 \left( 2R^2 W^* + \alpha h \dfrac{\partial U}{\partial x} + 2\dot{h}_0 \right)$ |
| Equation (160) | $\dfrac{\partial S}{\partial t} = 0$ |

Table 1: Splitting.

mann solver, except that the term $\partial(hP)/\partial x$ is treated as a source term by a central finite difference. The interface speed of the Rusanov solver is calculated as the maximum value between the left and right cells of the hydraulic characteristics $U \pm \sqrt{gh}$ since the slow terms do not include the acoustic part of the system (note that $R \exp[-M^2] < 1$).

The fast terms in the second explicit stage of the IMEX scheme are calculated by a forward Euler method.

The time step is calculated by a standard Courant-Friedrichs-Levy (CFL) condition $\Delta t = C \Delta x / c_{\max}$ where $C$ is the Courant number, $\Delta t$ the time step, $\Delta x$ the cell size and $c_{\max}$ is the maximum value of the characteristic velocities (164). In practice, it is convenient to take $c_{\max} = \max(U \pm \sqrt{gh + a^2})$ which is very close to $c_{\max} = a$. A Courant number equal to 0.8 was used in the computations.

If $\alpha = 1$, the fifth equation (for the variable $S$) is not solved, being useless.

### *5.3. Soliton on a flat bottom in the compressible case*

This numerical scheme is used to simulate the propagation of a soliton in water of constant depth. The attenuation of a solitary wave with an initial amplitude of 4.79 m propagating in a large depth of $h_\infty = 4000$ m is studied with $\overline{F}_\infty \simeq 1.005$ and $M_\infty \simeq 0.132$. The wave length, estimated between the two inflection points, is $\lambda \simeq 175$ km. For a real-time simulation of 2 h 36 min in a periodic box of length 1600 km, the diminution of the soliton's amplitude is of 1.04 % for a cell size $\Delta x = 8$ km ($\lambda/\Delta x \simeq 22$) and decreases to 0.02 % for $\Delta x = 2$ km ($\lambda/\Delta x \simeq 88$) and to 0.006 % for $\Delta x = 1$ km ($\lambda/\Delta x \simeq 175$).

With the same initial amplitude, depth, Froude and Mach numbers, in a non-periodic domain of 2400 km, after a real-time simulation of 5 h 12 min in the reference frame of the soliton, the amplitude of the soliton has decreased by only 1.1 %, 0.13 %, 0.022 % and 0.009 % with $\Delta x = 6$ km ($\lambda/\Delta x \simeq 29$), $\Delta x = 3$ km ($\lambda/\Delta x \simeq 58$), $\Delta x = 1.5$ km ($\lambda/\Delta x \simeq 117$) and $\Delta x = 1$ km ($\lambda/\Delta x \simeq 175$) respectively. In this case, the computational domain is extended by 300 cells on each side where initially $h$, $U$ and $P$ are equal to their respective values at the closest boundary of the domain and where initially $W = 0$. These extensions prevent the appearance of small perturbations at the edges. There is no need for a relaxation in these cells because of the choice of the reference frame (the position of the soliton is fixed).

With a cell size such that $\lambda/\Delta x$ is of the order of 100 or even 50, the numerical attenuation is negligible even for a very long simulation. The numerical values chosen above being representative of a typical tsunami in the ocean, a cell size of about 1 km is thus likely to be appropriate for the simulation of a tsunami in a deep ocean of approximately constant depth.

### *5.4. Waves train over a submerged bar*

The quasi-incompressible model is tested on the classical experiments of Beji & Battjes (1993) [63] on wave propagation over a submerged bar. In these experiments, waves were generated in a flume with a length of 37.7 m, a width of 0.8 m and a height of 0.75 m. The submerged bar was trapezoidal and had an upslope of 1/20 followed by a 2 m horizontal crest and then a 1/10 downslope. The still water depth was 0.4 m in the deep region and 0.1 m over the horizontal part of the bar (see figure 8). At the end of the flume opposite to the wave generator, a beach was used to serve as a wave absorber. The free surface elevations were measured at 8 wave gages, numbered from 1 to 8 on the figure 8. The first wave gage was located at the end of the constant-depth section, the second one was placed 1 m before the horizontal part of the bar and the following gages were placed at 1 m intervals. Wave gage 8 was thus at the downslope toe. Complete details of the experiments can be found in Beji & Battjes (1993) [63].

Several series of experiments were run by Beji & Battjes (1993) [63] with monochromatic waves or with irregular waves, in the case of non-breaking waves, spilling waves or plunging waves, with two different peak periods. The experiments with non-breaking monochromatic waves with frequencies of 0.4 Hz (precisely 0.396 Hz) and 1.0 Hz (precisely 0.99 Hz) were selected for numerical simulation in the present work. Cases of spilling monochromatic waves and of spilling irregular waves were simulated by Richard *et al.* (2019) [64] and Duran & Richard (2020) [65] respectively, although in both cases with an incompressible

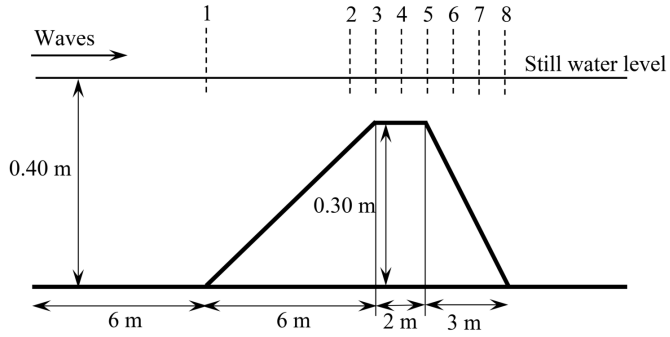


Figure 8: Sketch of the experimental configuration of Beji & Battjes (1993) [63].

non-hyperbolic model. As the goal was to test the hyperbolic version of the dispersive model and the new treatment of the bathymetric terms, the non-breaking case was sufficient. If necessary, shear, turbulence and breaking effects can be included in a similar way as by Kazakova & Richard (2019) [48].

These experiments aimed at investigating the phenomenon of high frequency energy generation as waves travel over submerged bars. Wave breaking was found to be a secondary effect in this process. The dominant physical effect takes place during the shoaling process and the de-shoaling phenomenon in the deepening region (Beji & Battjes 1993) [63]. These experiments are thus highly relevant to test the dispersive properties, the non-linear effects and the treatment of the bathymetry in the model.

Sinusoidal waves were generated with the relaxation method of Madsen *et al.* (2003) [66] in a wavemaker layer before the computational domain. At the other end of the 24 m long domain, the waves were absorbed in a 10 m long sponge layer with similar relaxation techniques. In some simulations a beach was present at the end of the domain, as in the experiments, but this changed nothing to the results. Since inevitably the phase of the generated waves is different than in the experiments, the results of the first wave gage were used to correct the phase. The same time shift was used thereafter at every wave gages to obtain a fair comparison. Grid convergence is reached with 2400 cells in the case of a frequency of 0.4 Hz and with 3600 cells in the case of a frequency of 1.0 Hz (although numerical convergence is almost obtained with 1200 and 2400 cells respectively).

In the case of a frequency of 0.4 Hz, the results of the quasi-incompressible model with improved dispersive properties with $\alpha = 1.159$ and $a = 30\,\mathrm{m}\cdot\mathrm{s}^{-1}$ on an arbitrary bathymetry are compared to the experimental results in figure 9, at wave gages 1 (a), 3 (b), 5 (c), 6 (d), 7 (e) and 8 (f). With this value of the sound velocity, the Mach number is always smaller than 0.1 which means that the difference with the incompressible case is negligible. The agreement is very good for all gages, including the last ones where the generation of high frequency energy due to the nonlinear interactions taking place in the de-shoaling phenomenon in deepening water is highly demanding for a numerical model.

When the dispersive properties are not improved, the agreement is very good until wave gage 5 but a discrepancy appears in the deepening part of the bar, at wave gage 6, and this discrepancy becomes increasingly large thereafter. Results at wave gage 8 are presented in figure 10 for one wave period, where the black dots are the experimental measurements of Beji & Batjjes (1993) [63]. In figure 10(a), the blue curve is the standard quasi-incompressible model with no improved dispersion, the red curve is the quasi-incompressible model with improved dispersion ($\alpha = 1.159$) and arbitrary bathymetry and the green curve is the quasi-incompressible model with improved dispersion ($\alpha = 1.159$) and a mild slope. In all cases, the value $a = 30\,\mathrm{m}\cdot\mathrm{s}^{-1}$ is used. When the dispersive properties are not improved, the discrepancy is very large. It is necessary to use the model with improved dispersion to obtain a good accuracy. However the results are already very good with the mild slope approximation. The more complex model with all bathymetric terms improves only marginally the accuracy of the results.

In figure 10(b) and 10(c), the effect of artificial reduction of the sound velocity is evaluated for the quasi-incompressible model with improved dispersive properties and arbitrary bathymetry. In figure 10(b), the red curve is the case $\alpha = 1.159$ and $a = 30\,\mathrm{m}\cdot\mathrm{s}^{-1}$, the green curve is the case $\alpha = 1.17$ and $a = 9.9\,\mathrm{m}\cdot\mathrm{s}^{-1}$ and the blue curve is the case $\alpha = 1.183$ and $a = 6.6\,\mathrm{m}\cdot\mathrm{s}^{-1}$. These values were discussed in §4.2.2. In all cases, the agreement is very good. For $a = 30\,\mathrm{m}\cdot\mathrm{s}^{-1}$, the properties are similar to the incompressible case. Decreasing the sound velocity to $a = 6.6\,\mathrm{m}\cdot\mathrm{s}^{-1}$ entails only a slight decrease of the accuracy. On the other hand, the computational time is considerably reduced. Compared to the case $a = 30\,\mathrm{m}\cdot\mathrm{s}^{-1}$, using exactly the same code, the same configuration, except for the value of $a$, on the same computer and with the same physical time, the computational time was divided by 2.9 using $a = 9.9\,\mathrm{m}\cdot\mathrm{s}^{-1}$ and was divided by 4.3 using $a = 6.6\,\mathrm{m}\cdot\mathrm{s}^{-1}$. This is due to the fact that the time step is calculated with a CFL condition based on the characteristic velocities, which are almost equal to $a$ since the sound velocity is much larger than all other velocities. Consequently the ratios of the computational times are very close to the ratios of the sound velocities, which are respectively 3.0 and 4.5.

In figure 10(c), $\alpha = 1.159$ in all cases. The red curve is the case $a = 30\,\mathrm{m}\cdot\mathrm{s}^{-1}$, the green curve is the case $a = 9.9\,\mathrm{m}\cdot\mathrm{s}^{-1}$ and the blue curve is the case $a = 6.6\,\mathrm{m}\cdot\mathrm{s}^{-1}$. This time, the accuracy is equivalent with a smaller sound velocity and thus with a faster computational time. As above, the computational time was divided by 2.9 using $a = 9.9\,\mathrm{m}\cdot\mathrm{s}^{-1}$ and was divided by 4.3 using $a = 6.6\,\mathrm{m}\cdot\mathrm{s}^{-1}$.

The comparisons of the numerical simulations with the experimental results in the case of a frequency of 1.0 Hz are presented in figure 11 (a) and (b) at wave gage 1, (c) and (d) at wave gage 3, (e) and (f) at wave gage 7 and (g) and

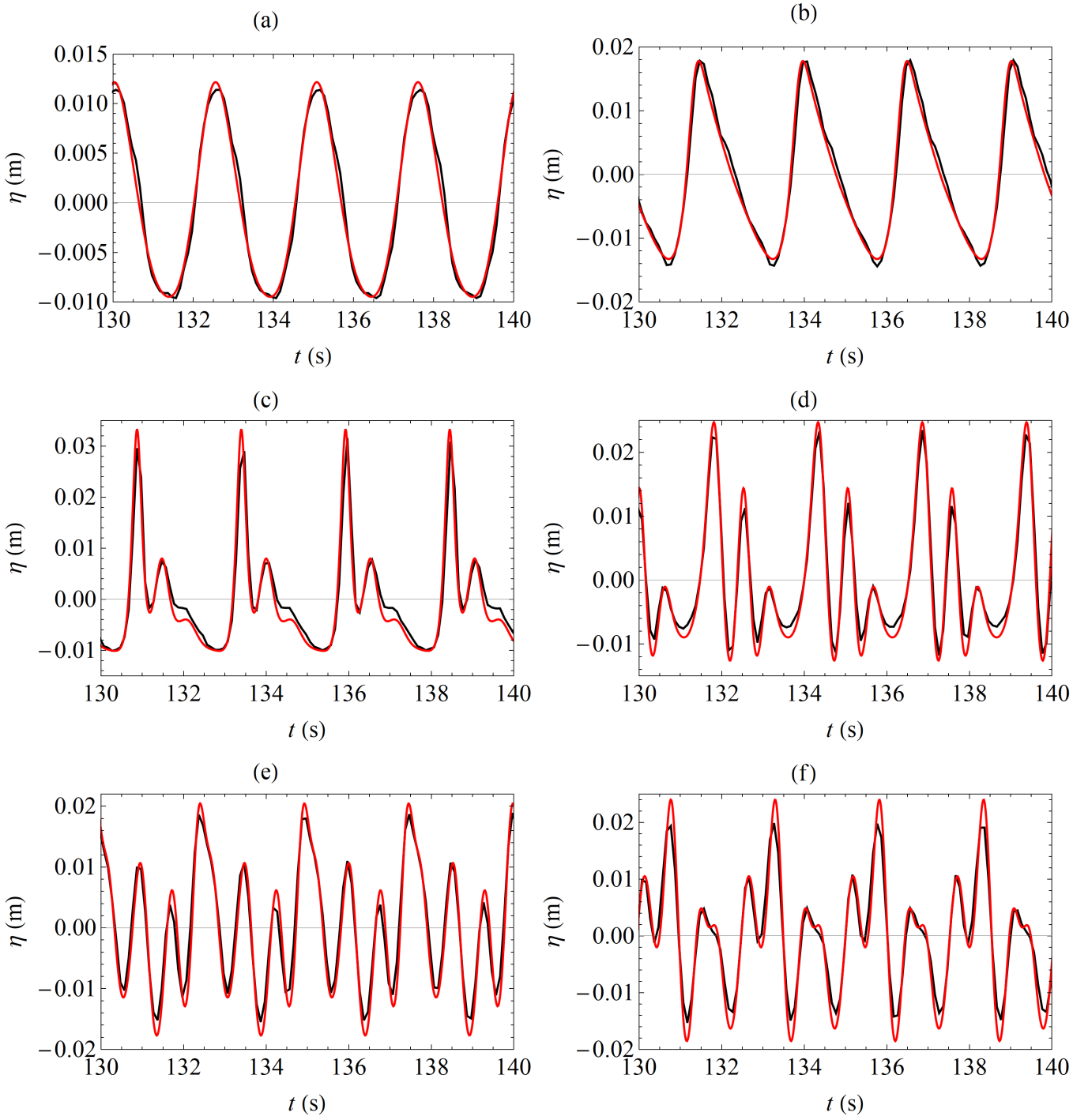


Figure 9: Comparisons of the quasi-incompressible model with improved dispersive properties ($\alpha = 1.159$, $a = 30\,\mathrm{m}\cdot\mathrm{s}^{-1}$, red curves) with the experimental results of Beji & Battjes (1993) [63] at the wave gages 1 (a), 3 (b), 5 (c), 6 (d), 7 (e) and 8 (f) (black curves).

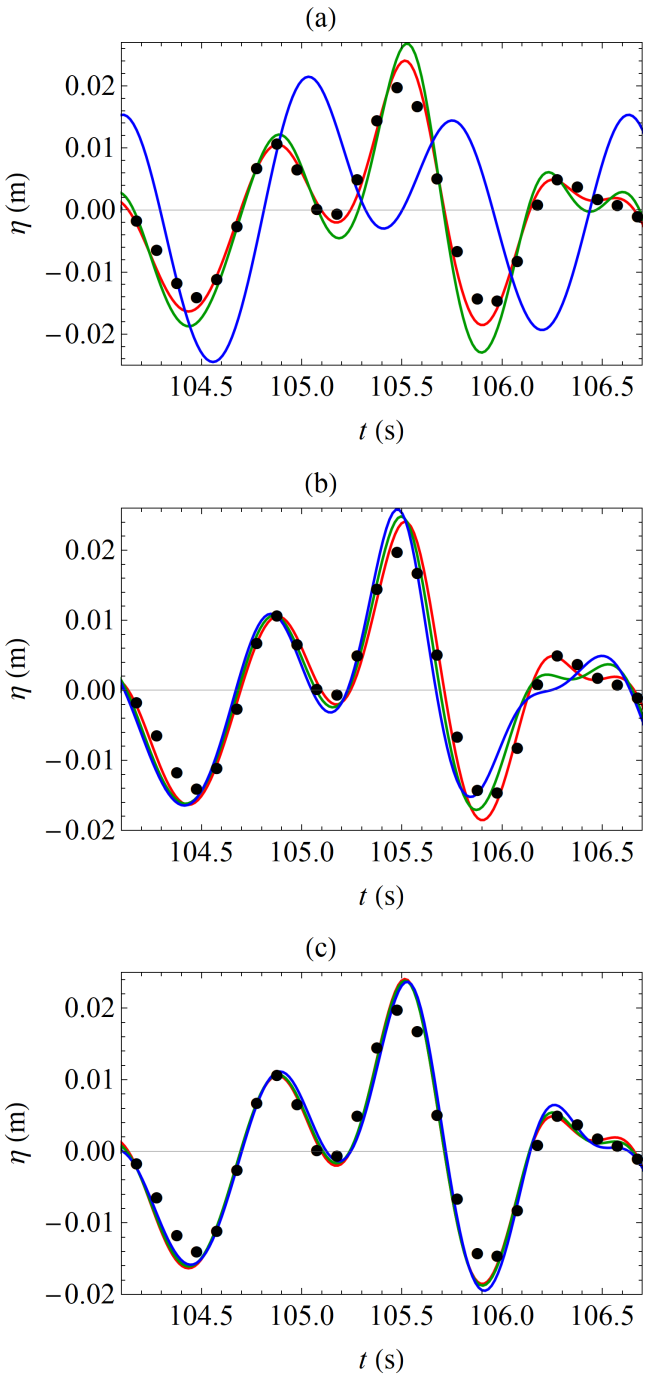


Figure 10: Comparisons of the quasi-incompressible model with the experimental results of Beji & Battjes (1993) [63] at wave gage 8 (dots). Red curve: model with improve dispersive properties ($\alpha = 1.159$, $a = 30\,\mathrm{m}\cdot\mathrm{s}^{-1}$) on an arbitrary bathymetry. (a) blue curve: model with standard dispersive properties ($\alpha = 1$, $a = 30\,\mathrm{m}\cdot\mathrm{s}^{-1}$); green curve: model with improved dispersive properties ($\alpha = 1.159$, $a = 30\,\mathrm{m}\cdot\mathrm{s}^{-1}$) on a mild slope. (b) blue curve: $\alpha = 1.183$ and $a = 6.6\,\mathrm{m}\cdot\mathrm{s}^{-1}$; green curve: $\alpha = 1.17$ and $a = 9.9\,\mathrm{m}\cdot\mathrm{s}^{-1}$. (c) blue curve: $\alpha = 1.159$ and $a = 6.6\,\mathrm{m}\cdot\mathrm{s}^{-1}$; green curve: $\alpha = 1.159$ and $a = 9.9\,\mathrm{m}\cdot\mathrm{s}^{-1}$.

(h) at wave gage 8, for a duration of one period. All values are shifted in time to coincide at wave gage 1. The dots are the experimental measurements of Beji & Batjjes (1993) [63]. The red curve is the result of the simulation obtained using the model with improved dispersive properties on an arbitrary bathymetry with $\alpha = 1.159$ and $a = 30\,\mathrm{m}\cdot\mathrm{s}^{-1}$. In figure 11 (a), (c), (e) and (g), the green curve is obtained with $\alpha = 1.159$ and $a = 9.9\,\mathrm{m}\cdot\mathrm{s}^{-1}$ and the blue curve with $\alpha = 1.159$ and $a = 6.6\,\mathrm{m}\cdot\mathrm{s}^{-1}$. In figure 11 (b), (d), (f) and (h), the blue and green curves are the results obtained using the model with standard dispersive properties ($\alpha = 1$), the blue curve with $a = 30\,\mathrm{m}\cdot\mathrm{s}^{-1}$ and the green curve with a reduced sound velocity $a = 6.6\,\mathrm{m}\cdot\mathrm{s}^{-1}$.

For the model with standard dispersive properties, the discrepancy is very large at all wave gages following the first (see figure 11 (d), (f) and (h)) and it is even worst with a reduced sound velocity. For the model with improved dispersive properties, the agreement is good except at wave gage 8 where there is an important discrepancy. At this wave gage, a model with more accurate dispersive properties is needed to obtain a good agreement, due to the very high frequencies that appear in the system. With a reduced sound velocity, the accuracy is actually slightly improved (figure 11 (c), (e) and (g)) and, more importantly, the calculation is much faster. As above, compared to the case with $a = 30\,\mathrm{m}\cdot\mathrm{s}^{-1}$ (everything else being exactly the same), the computational time is divided by 2.9 with $a = 9.9\,\mathrm{m}\cdot\mathrm{s}^{-1}$ and by 4.3 with $a = 6.6\,\mathrm{m}\cdot\mathrm{s}^{-1}$.

This remarkable effect can be explained by figure 6(a): the range in terms of $kh_0$ where the phase velocity keeps an accurate value is increased if the Mach number is increased. This effect is particular to the model with improved dispersive properties. In the case of the standard model, the dispersive properties deteriorate if the Mach number is increased and a faster computation is obtained at the cost of a smaller accuracy. On the contrary, in the case of the model with improved dispersive properties, it is possible to obtain both faster computation and better accuracy. In particular the accuracy is better than what can be obtained with an incompressible model. However the sound velocity cannot be indefinitely reduced and it seems unreasonable to increase the Mach number much above 0.3.

These test cases of Beji & Battjes (1993) [63] show that it is necessary to use the model with improved dispersive properties to obtain high accuracy in deepening water. This is the same conclusion as found by Beji & Battjes (1994) [67] from a comparison between the Boussinesq model of Peregrine (1967) [2] and the Boussinesq model with improved dispersion characteristics and mild slope of Madsen & Sørensen (1992) [9]. The mild slope approximation gives a simpler model, which is sufficient to produce accurate results, the full model with all bathymetric terms giving a slight improvement. Use of an artificial reduction in sound velocity can lead to a large decrease of the computational time with the same accuracy or with even a slightly better accuracy.

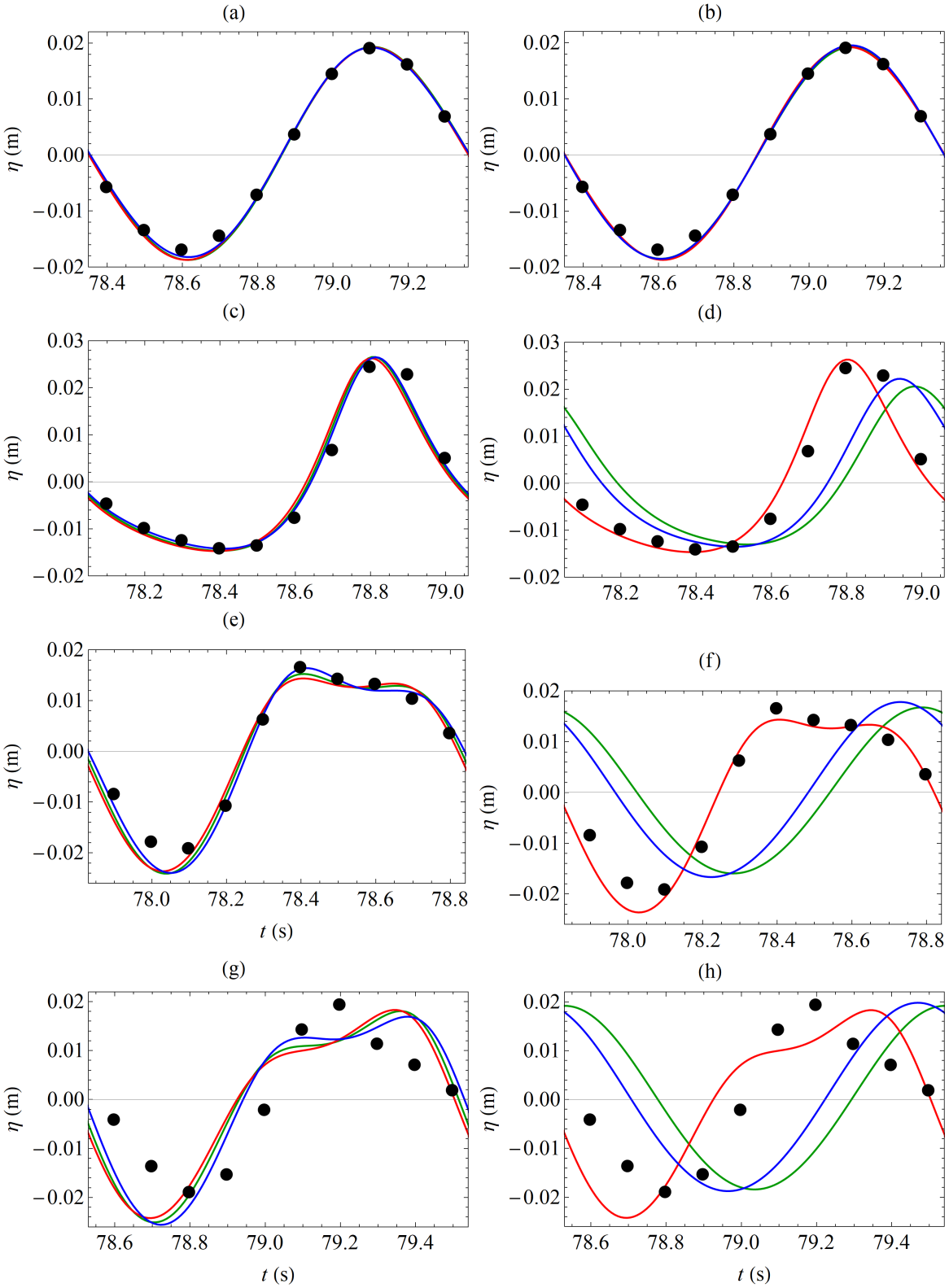


Figure 11: Comparisons of the quasi-incompressible model with the experimental results of Beji & Battjes (1993) [63] (dots) for a frequency of 1.0 Hz. (a) and (b): wave gage 1; (c) and (d): wave gage 3; (e) and (f): wave gage 7; (g) and (h): wave gage 8. (a), (c), (e) and (g): $\alpha = 1.159$, $a = 30\,\mathrm{m}\cdot\mathrm{s}^{-1}$( red curve); $\alpha = 1.159$, $a = 9.9\,\mathrm{m}\cdot\mathrm{s}^{-1}$ (green curve); $\alpha = 1.159$, $a = 6.6\,\mathrm{m}\cdot\mathrm{s}^{-1}$ (blue curve). (b), (d), (f) and (h): $\alpha = 1.159$, $a = 30\,\mathrm{m}\cdot\mathrm{s}^{-1}$ (red curve); $\alpha = 1.0$, $a = 30\,\mathrm{m}\cdot\mathrm{s}^{-1}$ (blue curve); $\alpha = 1.0$, $a = 6.6\,\mathrm{m}\cdot\mathrm{s}^{-1}$ (green curve).

*5.5. Compressible correction to the propagation of a tsunami*

The model is used to simulate a tsunami generated by an earthquake in a 1D-case. The goal is to assess the effect of compressibility on the results. This is by no means a simulation of a real tsunami although it is loosely inspired by a simulation of the Tohoku 2011 event by Abdolali & Kirby (2017) [37] who used a seabed motion reconstruction from Grilli *et al.* (2013) [33].

The bathymetry used for the numerical calculations is shown in figure 12(a) as the variations of $b = -h_0$ with the abscissa $x$ (taking the horizontal datum at the still water level). The domain is 2300 km long with two sponge layers on each side to absorb the waves. The coast is on the left of the figure in the direction of negative abscissas. The sponge layer in this direction has a constant depth of 200 m and 100 cells. The sponge layer on the right of the figure has 200 cells and a constant depth of 6000 m. In some parts of the domain, notably in the oceanic trench for $0 \leqslant x \leqslant 400$ km, the variation of the bottom in space is rapid enough to justify the use of a non-uniform mesh. The minimum size of the cells is 180 m and the maximum size is 1000 m for a total of 2890 cells. This mesh resolution was sufficient to achieve grid convergence because a numerical simulation with a maximum cell size of 500 m for a total of 4893 cells gave the same result.

The first test was the "sea at rest". The numerical scheme was found to preserve the equilibrium state, which confirms its well-balanced property.

In the following test, a 1D-tsunami was simulated. The tsunami is initiated by a seabed movement caused by an earthquake. In the numerical simulation the tsunami is generated by a moving bottom. As shown by Dutykh *et al.* (2006) [68], this method is preferable to the more usual method of translating the maximum bottom displacement as an initial condition on the surface elevation. The maximum value $\Delta b_{\max}$ of the variation $\Delta b$ of the bottom is shown in Figure 12(b). Since no real simulation is intended, the movement of the bottom is supposed to follow the simple function

$$h_0(x,t) = h_0(x,0) - \frac{\Delta b_{\max}(x)}{2}\left(1 + \tanh\frac{t-\tau/2}{\tau_m}\right) \quad (172)$$

Other functions were proposed by Dutykh & Dias (2007) [69]. Different values of $\tau$ and $\tau_m$ were used. The most important parameter is $\tau_m$ which determines the rapidity of the seabed movement. If $\tau_m$ is small ($\tau_m \leqslant 20$ s in the present case), the fast movement of the bottom generates acoustic waves with a significant amplitude of non-hydrostatic pressure although the effect on the water elevation is very small. This is due to the values of $\partial h_0/\partial t$ which are large if $\tau_m$ is small. For larger values of $\tau_m$, no significant acoustic waves are generated by the bottom movement. The value of $\tau$ must be chosen large enough to give no discontinuity of $h_0$ at the initial time. The following tests were obtained with the values $\tau_m = 40$ s and $\tau = 600$ s for which almost no acoustic waves are generated. Note that, in the cases where there are acoustic waves, they behave as described in §3.2 with a cutoff frequency and a reflection on small depths.

The movement of the seabed generates two waves, one propagating toward the coast and another propagating in the opposite direction. These waves at different times (1520 s, 2534 s, 3886 s and 8955 s) are shown on Figure 13(a). The tsunami propagating shoreward steepens rapidly and its amplitude increases quickly. In the other wave, a train of secondary waves is generated during the propagation, behind the main hump (Figure 13).

A simulation was performed with the mild-slope equations for a comparison to the equations with an arbitrary bathymetry. The difference is 0.6 % for the maximum amplitude and is negligible for the arrival time. The bathymetric terms of $O(\varepsilon^2)$ have thus a very small effect on the tsunami propagation. Since the mild-slope equations are much simpler, they can be used with a very good approximation if the slopes are not very steep.

The effect of compressibility is studied by the comparison between the results given by the compressible model and by the quasi-incompressible model. The water elevation at $x = 2000$ km is presented in Figure 13(b) for the system with improved dispersive properties and $\alpha = 1.19$ (in both cases, the compressible case is in red and the quasi-incompressible case in black). The arrival time in the compressible case is 42 s later than in the quasi-incompressible case. This value is very close to the time lag found by Abdolali & Kirby (2017) [37] (48 s) in a very similar case. The inclusion of compressibility in the model leads to a significant reduction of the velocity of the tsunami and to an increase of the arrival time.

## 6. Conclusion

An extension of the Boussinesq-type models is proposed for weakly compressible flows. The depth-averaged density is variable. Since the shallow-water assumption implies that the system is weakly dispersive, the effect of the non-hydrostatic part of the pressure on the density variations is negligible and the average density variations are due to the variations of the hydrostatic pressure caused by the changes of the water depth. In the general case of an arbitrary bathymetry as well as in the particular case of a mild-slope bottom, the system is fully nonlinear, hyperbolic, with four equations, and admits an exact energy conservation equation. The linear dispersive properties are consistent with the linear theory of compressible fluids at the long-wave limit. In particular, the compressibility decreases the phase velocity of the gravity waves. The equations include the case of a mobile bottom to simulate the generation of tsunamis by earthquakes and the vertical movements of the seabed.

As a particular case of this compressible model, a quasi-incompressible model is obtained at the limit where the Mach number goes to zero. This quasi-incompressible model is a hyperbolic approximation of the fully nonlinear Serre-Green-Naghdi equations with a new treatment of the bathy-

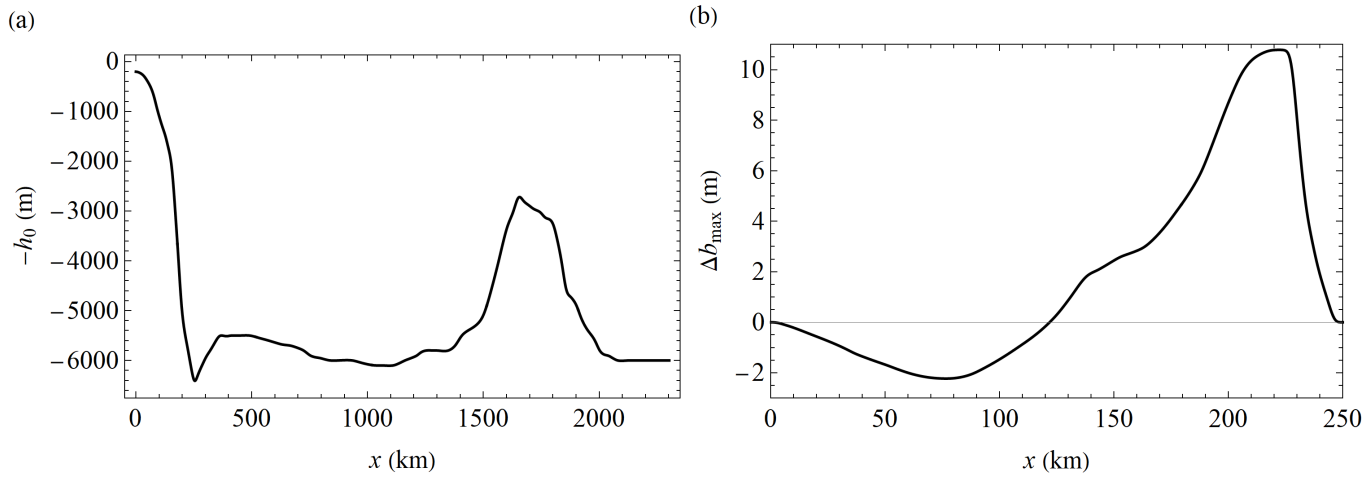


Figure 12: (a) Bathymetry and (b) maximum seabed vertical displacement.

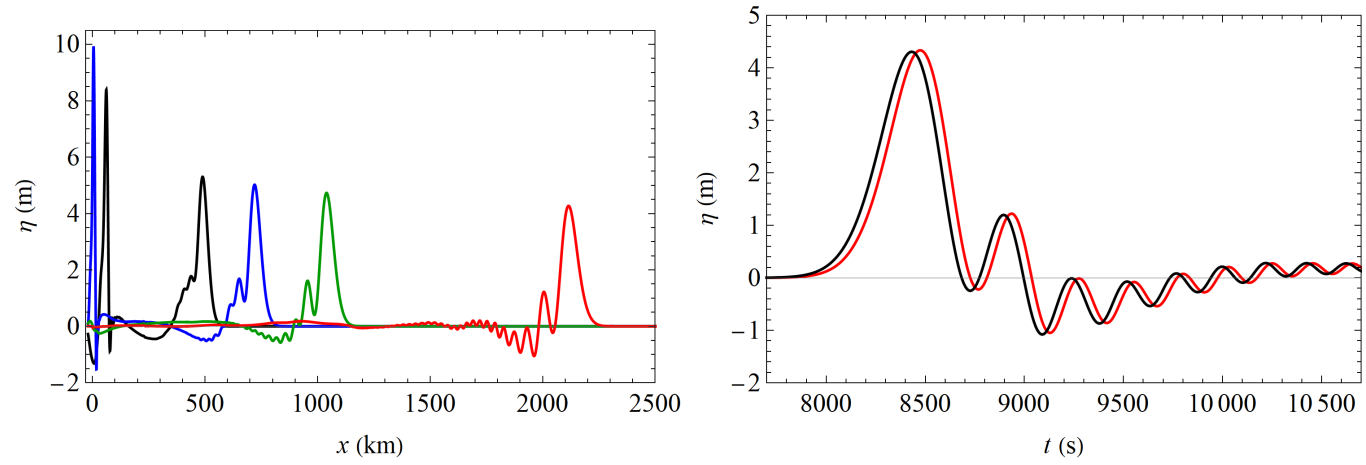


Figure 13: (a) Water elevation at $t = 1520\,\mathrm{s}$ (black), $t = 2534\,\mathrm{s}$ (blue), $t = 3886\,\mathrm{s}$ (green), $t = 8955\,\mathrm{s}$ (red). (b) Water elevation at $x = 2000\,\mathrm{km}$ for the compressible case equations (red curve) and the quasi-incompressible case equations (black curve).

metric terms which gives a four-equation system on an arbitrary bathymetry with an exact equation of energy conservation. The sound velocity can be artificially reduced to reduce the computational time as long as the Mach number $\sqrt{gh}/a \leqslant 0.1$.

The adaptation to the compressible case of the method of Bonneton *et al.* (2011) [13], supplemented by an original method specific to the compressible case, leads to a model with improved dispersive properties. This five-equation model is also hyperbolic and fully nonlinear. The drawback of this method, as in the incompressible case, is that conservation of energy is not satisfied exactly but only asymptotically. This method is used both for the quasi-incompressible model and for the compressible model. In the specific case of the compressible model, using these two methods together gives highly accurate values of the phase and group velocities for the characteristic tsunamis wavelengths.

In the quasi-incompressible case, a remarkable property of the model with improved dispersive properties is that the sound velocity can be decreased much more than for the model with standard dispersion. The Mach number can be artificially increased to 0.2 or even 0.3 with the same or slightly better accuracy. This method enables the computational time to be reduced even further. In this respect, the accuracy can be slightly improved compared to the incompressible Serre-Green-Naghdi model with improved dispersive properties of Bonneton *et al.* (2011) [13].

The numerical scheme used to solve the system is based on a splitting between a slow part, solved explicitly, and a fast part, solved implicitly. Since the implicit part of the scheme does not involve the resolution of a global linear system, its computational cost is very cheap. Numerical simulations were obtained for a soliton in the case of a constant depth. The quasi-incompressible model has been validated by comparison to results of Beji & Battjes (1993) [63] for monochromatic non-breaking waves. The model with improved dispersive properties is necessary to obtain accurate results in the de-shoaling deepening part, but its mild-slope version gives already a good agreement. An important artificial reduction of the sound velocity, and thus of the computational cost, is possible with no decrease of accuracy.

The compressible model was solved in the case of a variable bottom, for a 1D-tsunami generated by a mobile seabed. The equations predict a later arrival time of the tsunami due to compressibility effects. This system of equations is a first step toward a complete model for tsunamis, which will need the inclusion, in particular, of the elastic waves in the solid bottom, of the Coriolis forces, and of shear and possible breaking effects near the coasts, before realistic 2D-applications.

**Acknowledgments** The author thanks Arnaud Duran and Jean-Paul Vila for helpful suggestions and discussions.

Funding: This work was supported by the French National program LEFE (Les Enveloppes Fluides et l'Environnement).

## References

[1] J. Boussinesq, Théorie des ondes et des remous qui se propagent le long d'un canal rectangulaire horizontal, en communiquant au liquide contenu dans ce canal des vitesses sensiblement pareilles de la surface au fond., J. mathématiques pures et appliquées (1872) 55–108.

[2] D. H. Peregrine, Long waves on a beach, J. Fluid Mech. 27 (4) (1967) 815–827.

[3] F. Serre, Contribution à l'étude des écoulements permanents et variables dans les canaux, La Houille Blanche (6) (1953) 830–872.

[4] C. H. Su, C. S. Gardner, Korteweg-de vries equation and generalizations. iii. derivation of the korteweg-de vries equation and burgers equation, J. Math. Phys. 10 (3) (1969) 536–539.

[5] A. E. Green, N. Laws, P. Naghdi, On the theory of water waves, Proc. R. Soc. Lond. A 338 (1612) (1974) 43–55.

[6] A. Green, P. Naghdi, A derivation of equations for wave propagation in water of variable depth, J. Fluid Mech. 78 (2) (1976) 237–246.

[7] D. Lannes, The water waves problem: mathematical analysis and asymptotics, Vol. 188, American Mathematical Soc., 2013.

[8] J. T. Kirby, Boussinesq models and their application to coastal processes across a wide range of scales, J. Waterw. Port Coast. 142 (6) (2016) 03116005.

[9] P. A. Madsen, O. R. Sørensen, A new form of the boussinesq equations with improved linear dispersion characteristics. part 2. a slowly-varying bathymetry, Coast. Eng. 18 (3-4) (1992) 183–204.

[10] O. Nwogu, Alternative form of boussinesq equations for nearshore wave propagation, J. Waterw. Port Coast. 119 (6) (1993) 618–638.

[11] G. Wei, J. T. Kirby, S. T. Grilli, R. Subramanya, A fully nonlinear boussinesq model for surface waves. part 1. highly nonlinear unsteady waves, J. Fluid Mech. 294 (1995) 71–92.

[12] A. B. Kennedy, J. T. Kirby, Q. Chen, R. A. Dalrymple, Boussinesq-type equations with improved nonlinear performance, Wave Motion 33 (3) (2001) 225–243.

[13] P. Bonneton, F. Chazel, D. Lannes, F. Marche, M. Tissier, A splitting approach for the fully nonlinear and weakly dispersive green–naghdi model, J. Comput. Phys. 230 (4) (2011) 1479–1498.

[14] F. Chazel, D. Lannes, F. Marche, Numerical simulation of strongly nonlinear and dispersive waves using a green–naghdi model, J. Sci. Comput. 48 (1) (2011) 105–116.

[15] Y. Agnon, P. A. Madsen, H. Schäffer, A new approach to high-order boussinesq models, J. Fluid Mech. 399 (1999) 319–333.

[16] M. F. Gobbi, J. T. Kirby, G. Wei, A fully nonlinear boussinesq model for surface waves. part 2. extension to o (kh) 4, J. Fluid Mech. 405 (2000) 181–210.

[17] P. A. Madsen, H. Bingham, H. Liu, A new boussinesq method for fully nonlinear waves from shallow to deep water, J. Fluid Mech. 462 (2002) 1–30.

[18] P. Lynett, P. L.-F. Liu, A two-layer approach to wave modelling, Proc. R. Soc. A 460 (2049) (2004) 2637–2669.

[19] Z. Liu, K. Fang, Y. Cheng, A new multi-layer irrotational boussinesq-type model for highly nonlinear and dispersive surface waves over a mildly sloping seabed, J. Fluid Mech. 842 (2018) 323–353.

[20] M. Brocchini, A reasoned overview on boussinesq-type models: the interplay between physics, mathematics and numerics, Proc. R. Soc. A 469 (2160) (2013) 20130496.

[21] M. Antuono, V. Liapidevskii, M. Brocchini, Dispersive nonlinear shallow-water equations, Stud. Appl. Math. 122 (1) (2009) 1–28.

[22] N. Favrie, S. Gavrilyuk, A rapid numerical method for solving serre–green–naghdi equations describing long free surface gravity waves, Nonlinearity 30 (7) (2017) 2718–2736.

[23] V. Duchêne, Rigorous justification of the favrie–gavrilyuk approximation to the serre–green–naghdi model, Nonlinearity 32 (10) (2019) 3772.
[24] C. Escalante, M. Dumbser, M. Castro, An efficient hyperbolic relaxation system for dispersive non-hydrostatic water waves and its solution with high order discontinuous galerkin schemes, J. Comput. Phys. 394 (2019) 385–416.
[25] C. Escalante, T. Morales de Luna, A general non-hydrostatic hyperbolic formulation for boussinesq dispersive shallow flows and its numerical approximation, J. Sci. Comput. 83 (3) (2020) 1–37.
[26] C. Bassi, L. Bonaventura, S. Busto, M. Dumbser, A hyperbolic reformulation of the serre-green-naghdi model for general bottom topographies, Comput. Fluids 212 (2020) 104716.
[27] G. E. Hill, Factors controlling the size and spacing of cumulus clouds as revealed by numerical experiments, J. Atmos. Sci. 31 (3) (1974) 646–673.
[28] J. B. Klemp, R. B. Wilhelmson, The simulation of three-dimensional convective storm dynamics, J. Atmos. Sci. 35 (6) (1978) 1070–1096.
[29] W. C. Skamarock, J. B. Klemp, The stability of time-split numerical methods for the hydrostatic and the nonhydrostatic elastic equations, Mon. Weather Rev. 120 (9) (1992) 2109–2127.
[30] W. C. Skamarock, J. B. Klemp, A time-split nonhydrostatic atmospheric model for weather research and forecasting applications, J. Comput. Phys. 227 (7) (2008) 3465–3485.
[31] F. Auclair, L. Bordois, Y. Dossmann, T. Duhaut, A. Paci, C. Ulses, C. Nguyen, A non-hydrostatic non-boussinesq algorithm for free-surface ocean modelling, Ocean Model. 132 (2018) 12–29.
[32] Y. Yamazaki, K. F. Cheung, Z. Kowalik, Depth-integrated, non-hydrostatic model with grid nesting for tsunami generation, propagation, and run-up, Int. J. Numer. Meth. Fl. 67 (12) (2011) 2081–2107.
[33] S. T. Grilli, J. C. Harris, T. S. T. Bakhsh, T. L. Masterlark, C. Kyriakopoulos, J. T. Kirby, F. Shi, Numerical simulation of the 2011 tohoku tsunami based on a new transient fem coseismic source: Comparison to far-and near-field observations, Pure Appl. Geophys. 170 (6) (2013) 1333–1359.
[34] V. C. Tsai, J.-P. Ampuero, H. Kanamori, D. J. Stevenson, Estimating the effect of earth elasticity and variable water density on tsunami speeds, Geophys. Res. Lett. 40 (3) (2013) 492–496.
[35] S. Allgeyer, P. Cummins, Numerical tsunami simulation including elastic loading and seawater density stratification, Geophys. Res. Lett. 41 (7) (2014) 2368–2375.
[36] T. Baba, S. Allgeyer, J. Hossen, P. R. Cummins, H. Tsushima, K. Imai, K. Yamashita, T. Kato, Accurate numerical simulation of the far-field tsunami caused by the 2011 tohoku earthquake, including the effects of boussinesq dispersion, seawater density stratification, elastic loading, and gravitational potential change, Ocean Model. 111 (2017) 46–54.
[37] A. Abdolali, J. T. Kirby, Role of compressibility on tsunami propagation, J. Geophys. Res.-Oceans 122 (12) (2017) 9780–9794.
[38] A. Abdolali, U. Kadri, J. T. Kirby, Effect of water compressibility, sea-floor elasticity, and field gravitational potential on tsunami phase speed, Sci. Rep. 9 (1) (2019) 1–8.
[39] S. Watada, S. Kusumoto, K. Satake, Traveltime delay and initial phase reversal of distant tsunamis coupled with the self-gravitating elastic earth, J. Geophys. Res. Sol. Ea. 119 (5) (2014) 4287–4310.
[40] J. T. Kirby, F. Shi, B. Tehranirad, J. C. Harris, S. T. Grilli, Dispersive tsunami waves in the ocean: Model equations and sensitivity to dispersion and coriolis effects, Ocean Model. 62 (2013) 39–55.
[41] S. Glimsdal, G. K. Pedersen, C. B. Harbitz, F. Løvholt, Dispersion of tsunamis: does it really matter?, Nat. Hazards Earth Sys. 13 (6) (2013) 1507–1526.
[42] S. Watada, Tsunami speed variations in density-stratified compressible global oceans, Geophys. Res. Lett. 40 (15) (2013) 4001–4006.
[43] F. Ardhuin, T. H. Herbers, Noise generation in the solid earth, oceans and atmosphere, from nonlinear interacting surface gravity waves in finite depth, J. Fluid Mech. 716 (2013) 316–348.
[44] E. Renzi, F. Dias, Hydro-acoustic precursors of gravity waves generated by surface pressure disturbances localised in space and time, J. Fluid Mech. 754 (2014) 250–262.
[45] U. Kadri, M. Stiassnie, Generation of an acoustic-gravity wave by two gravity waves, and their subsequent mutual interaction, J. Fluid Mech. 735 (2013) R6.
[46] P. Sammarco, C. Cecioni, G. Bellotti, A. Abdolali, Depth-integrated equation for large-scale modelling of low-frequency hydroacoustic waves, J. Fluid Mech. 722 (2013) R6.
[47] A. Abdolali, J. T. Kirby, G. Bellotti, Depth-integrated equation for hydro-acoustic waves with bottom damping, J. Fluid Mech. 766 (2015) R1.
[48] M. Kazakova, G. L. Richard, A new model of shoaling and breaking waves: one-dimensional solitary wave on a mild sloping beach, J. Fluid Mech. 862 (2019) 552–591.
[49] V. Teshukov, Gas-dynamic analogy for vortex free-boundary flows, J. Applied Mechanics and Technical Physics 48 (3) (2007) 303–309.
[50] F. Pidduck, On the propagation of a disturbance in a fluid under gravity, Proc. R. Soc. Lond. A 83 (563) (1910) 347–356.
[51] R. A. Dalrymple, B. D. Rogers, A note on wave celerities on a compressible fluid, in: Coastal Engineering 2006: (In 5 Volumes), World Scientific, 2007, pp. 3–13.
[52] U. Kadri, Wave motion in a heavy compressible fluid: Revisited, Eur. J. Mech. B/Fluids 49 (2015) 50–57.
[53] D. R. Tappin, S. T. Grilli, J. C. Harris, R. J. Geller, T. Masterlark, J. T. Kirby, F. Shi, G. Ma, K. Thingbaijam, P. M. Mai, Did a submarine landslide contribute to the 2011 tohoku tsunami?, Mar. Geol. 357 (2014) 344–361.
[54] B. Rogers, M. Fujihara, A. G. Borthwick, Adaptive q-tree godunov-type scheme for shallow water equations, International Journal for Numerical Methods in Fluids 35 (3) (2001) 247–280.
[55] B. D. Rogers, A. G. Borthwick, P. H. Taylor, Mathematical balancing of flux gradient and source terms prior to using roe's approximate riemann solver, Journal of Computational Physics 192 (2) (2003) 422–451.
[56] Q. Liang, F. Marche, Numerical resolution of well-balanced shallow water equations with complex source terms, Adv. Water Resour. 32 (6) (2009) 873–884.
[57] A. Duran, F. Marche, A discontinuous galerkin method for a new class of green–naghdi equations on simplicial unstructured meshes, Appl. Math. Model. 45 (2017) 840–864.
[58] S. Tkachenko, Etude analytique et numérique d'un modèle dispersif des eaux peu profondes, Ph.D. thesis, Aix-Marseille Université (2020).
[59] H. Weller, S.-J. Lock, N. Wood, Runge–kutta imex schemes for the horizontally explicit/vertically implicit (hevi) solution of wave equations, J. Comput. Phys. 252 (2013) 365–381.
[60] F. Mesinger, et al., Forward-backward scheme, and its use in a limited area model, Contrib. Atmos. Phys. 50 (1977) (1977) 200–210.
[61] U. M. Ascher, S. J. Ruuth, R. J. Spiteri, Implicit-explicit runge-kutta methods for time-dependent partial differential equations, Appl. Numer. Math. 25 (2-3) (1997) 151–167.
[62] L. Pareschi, G. Russo, Implicit–explicit runge–kutta schemes and applications to hyperbolic systems with relaxation, J. Sci. Comput. 25 (1) (2005) 129–155.
[63] S. Beji, J. Battjes, Experimental investigation of wave propagation over a bar, Coast. Eng. 19 (1-2) (1993) 151–162.
[64] G. L. Richard, A. Duran, B. Fabrèges, A new model of shoaling and breaking waves. part 2. run-up and two-dimensional waves, J. Fluid Mech. 867 (2019) 146–194.
[65] A. Duran, G. L. Richard, Modelling coastal wave trains and wave breaking, Ocean Model. 147 (2020) 101581.
[66] P. A. Madsen, H. Bingham, H. Schäffer, Boussinesq-type formulations for fully nonlinear and extremely dispersive water waves: derivation and analysis, Proc. R. Soc. A 459 (2033) (2003) 1075–1104.

[67] S. Beji, J. Battjes, Numerical simulation of nonlinear wave propagation over a bar, Coast. Eng. 23 (1-2) (1994) 1–16.
[68] D. Dutykh, F. Dias, Y. Kervella, Linear theory of wave generation by a moving bottom, C. R. Acad. Sci. Paris, Ser. I 343 (7) (2006) 499–504.
[69] D. Dutykh, F. Dias, Water waves generated by a moving bottom, in: Tsunami and Nonlinear waves, Springer, 2007, pp. 65–95.